



POLITECNICO DI TORINO

DIPARTIMENTO DI INGEGNERIA MECCANICA E AEROSPAZIALE

MASTER OF SCIENCE IN MECHANICAL ENGINEERING

MASTER THESIS IN THERMAL AND HYDRAULIC MACHINES

**Assessment of the potentials of the
Adaptive Equivalent Consumption
Minimization Strategy application
to the energy management
of a Heavy-Duty Hybrid Electric Vehicle**

Academic Supervisors

Daniela Anna MISUL, Associate Professor

Claudio MAINO, PhD

Graduate:

Francesco CAPONE

260342

ACADEMIC YEAR 2020/2021

*To Nonno Nino,
a real mechanic.
Hope you are enjoying these results!*

Abstract

The present thesis aims at evaluating the advantages of the transformation of a conventional heavy-duty vehicle featured by a 4.5L diesel engine into a full hybrid version by applying an Adaptive - Equivalent Consumption Minimization Strategy (A-ECMS). A p2 parallel hybrid configuration has been simulated in a design optimization tool. The controller has been integrated within the simulation environment under multiple formulations, either extracted from the literature or proposed in innovative solutions. Simulations have been carried out in MATLAB and validated by comparing the results obtained by the Dynamic Programming optimization algorithm. In order to understand the behaviour of the vehicle in multiple traffic scenarios, WHVC (Worldwide Harmonized Vehicle Cycle), FTP-72 (Federal Test Procedure) and JC08 (Japan Cycle 08) have been used as driving cycles for the testing campaign.

Il presente lavoro di tesi ha lo scopo di comprendere i vantaggi derivanti dalla trasformazione di un veicolo pesante spinto da un propulsore termico diesel convenzionale 4.5L in un veicolo full-hybrid applicando l'algoritmo Adaptive - Equivalent Consumption Minimization Strategy (A-ECMS). Una configurazione ibrida parallela p2 è stata simulata, a tal fine, in un tool di ottimizzazione. Il controllore è stato successivamente integrato all'interno dell'ambiente di simulazione mediante formulazioni multiple, sia estratte dalla letteratura sia proponendo soluzioni innovative. Le simulazioni sono state eseguite con l'ausilio di MATLAB e validate confrontando i risultati ottenuti con l'ottimizzazione fornita dall'algoritmo di Programmazione Dinamica. Per comprendere il comportamento del veicolo in diversi scenari di traffico, i cicli guida WHVC, FTP-72 e JC08 sono stati utilizzati per la campagna di prova.

Acknowledgements

I would like to express my gratitude to my academic supervisor Prof. Daniela Anna Misul for her encouragement during this challenging year and for her support during these two years and a half at Politecnico. She is an amazing person capable of deal with student, in addition to being one of the best academics that I've ever met.

I would like to thank Claudio Maino PhD, for his assistance, patience and his helpful advises.

My deepest thank goes to my "brother in arm" Federico, more than a friend.

Our friendship (literally) survived until the end of this work carried out together. I wish you all the best for your future and I hope that our professional careers will cross each-other again.

A sincere thank goes to Carmela, an outstanding engineer and a wonderful friend.

Together with Federico we pass through this adventure, from the first day to such special occasion, and this is priceless !

Then I would like to express my profound gratitude to my parents, Antonio e Isabella, and to Bianca, my everlasting lighthouse.

Nevertheless I would like to thank Elena, Tommaso, Lorenzo, Serena, Nadia and Edward for their immense support, sincere friendship and for being my Turin family, especially during this last year far from home.

Last but not the least, I would sincerely acknowledge my chief, Luigi Pirillo, and the whole Iveco family, to give me the chance of not being just a final grade, but the sum of my mistakes which are, perhaps, the sum of my successes.

Frangar, non flectar !

Contents

1	Introduction	1
1.1	Powertrain electrification towards emission control	1
1.2	HEVs battery aspects in a growing circular economy	4
2	HEVs Control Strategies Optimization	8
2.1	Global Optimization Methods	10
2.1.1	Dynamic Programming	11
2.2	Instantaneous Optimization Methods	12
2.2.1	Equivalent Consumption Minimization Strategy - ECMS	12
2.2.2	Adaptive - ECMS	15
3	Model	17
3.1	Model Input	18
3.1.1	Architecture Definition	18
3.1.2	Electric machine	21
3.1.3	Battery pack and electrical energy accumulators	22
3.1.4	Internal Combustion Engine	24
3.1.5	Auxiliaries	24
3.1.6	Equivalence Factor definition by means of the Model-Based calibration	25
3.1.7	Driving Cycle	27
3.2	Data Processing	30
3.2.1	Pre-Processing Phase	30
3.3	Post Processing	35
4	Control Strategy	39
4.1	Instantaneous A-ECMS formulation	40
4.2	Periodic A-ECMS formulation	41
4.3	Hybrid A-ECMS formulation	45
5	Results	46
5.1	WHVC	47
5.2	FTP-72	53
5.3	JC08	59
6	Conclusions and Future works	65
6.1	Conclusions	65
6.2	Future works	66
	Bibliography	67

List of Figures

1.1	Hybrid electric vehicles classification [19]	2
1.2	Networking of control systems in the drivetrain - A. Actuator B. Sensor [17]	3
1.3	Roadmap for a zero impact mobility (*post Euro 6/VI)	4
1.4	Global passenger car sales forecast - Source: Boston Consulting Group	5
1.5	Automotive lithium-ion battery value chain	7
2.1	Charge-Sustaining vs. Charge-Depleting behaviour	8
2.2	Dynamic Programming Computational Grid	11
2.3	SOC penalty function	14
3.1	Parallel Hybrid configuration 1. Internal Combustion Engine; 2. Fuel Tank; 3. Electric Motor/Alternator; 4. Coupling devices; 5. Inverter; 6. Battery	19
3.2	P2 Parallel Hybrid configuration	19
3.3	Hybrid Operating Modes	21
3.4	Tector 5 engine series - Source: Iveco SpA workshop manual	24
3.5	Top to bottom: Pseudo-random, stratified sampling, Latin hypercube sampling and sampling based on Sobol sequences	26
3.6	Driving Cycle	27
3.7	World Harmonized Vehicle Cycle (WHVC)	27
3.8	Federal Test Procedure - 72	28
3.9	Japan Cycle 08	29
3.10	Battery pack	32
3.11	Battery equivalent model	33
3.12	SOC at the end of the mission	35
3.13	Example for $CO_{2,ttw}$ evaluation	36
3.14	Correction coefficient evaluation procedure	37
4.1	Periodic Adaptation Law	41
4.2	Sensitivity Analysis of the Periodic Controller Gains - T=20s and T=30s	43
4.3	Sensitivity Analysis of the Periodic Controller Gains - WHVC	44
4.4	Speed proportional gain for $s_{dis,0} = const$	45
5.1	SOC profile on WHVC - Best case scenario	47
5.2	Powerflow strategies on WHVC for different controllers - Best case scenario	48
5.3	Powerflow strategies comparison on WHVC	49
5.4	EMS comparison on WHVC - Instantaneous controller	50
5.5	Powerflow strategies and charging factor comparison on WHVC - Instantaneous controller	50

5.6	EMS comparison on WHVC - Periodic controller	51
5.7	Powerflow strategies on WHVC - Periodic controller	51
5.8	EMS comparison on WHVC - Hybrid controller	52
5.9	Powerflow strategies on WHVC - Hybrid controller	52
5.10	SOC profile on FTP72 - Best case scenario	53
5.11	Powerflow strategies on FTP72 for different controllers - Best case scenario	54
5.12	Powerflow strategies comparison on FTP72	55
5.13	EMS comparison on FTP72 - Instantaneous controller	56
5.14	Powerflow strategies on FTP72 - Instantaneous controller	56
5.15	EMS comparison on FTP72 - Periodic controller	57
5.16	Powerflow strategies on FTP72 - Periodic controller	57
5.17	EMS comparison on FTP72 - Hybrid controller	58
5.18	Powerflow strategies on FTP72 - Hybrid controller	58
5.19	SOC profile on JC08 - Best case scenario	59
5.20	Powerflow strategies on JC08 for different controllers - Best case scenario .	60
5.21	Powerflow strategies comparison on JC08	61
5.22	EMS comparison on JC08 - Instantaneous controller	62
5.23	Powerflow strategies on JC08 - Instantaneous controller	62
5.24	EMS comparison on JC08 - Periodic controller	63
5.25	Powerflow strategies on JC08 - Periodic controller	63
5.26	EMS comparison on JC08 - Hybrid controller	64
5.27	Powerflow strategies on JC08 - Hybrid controller	64

List of Tables

2.1	Dynamic Programming advantages and disadvantages	12
3.1	p2 architecture powerflow strategy	21
3.2	Battery input from optimization tool	32
3.3	Example for $CO_{2,ttw}$ correction and evaluation	36
3.4	Driving Cycle correction coefficients	38
5.1	$CO_{2,ttw}$ and Fuel economy reference values for each driving cycle	46
5.2	Best case scenario on WHVC test cycle	47
5.3	Worst case scenario on WHVC test cycle	49
5.4	Best case scenario on FTP72 test cycle	53
5.5	Worst case scenario on FTP72 test cycle	55
5.6	Best case scenario on JC08 test cycle	59
5.7	Worst case scenario on JC08 test cycle	61

Chapter 1

Introduction

1.1 Powertrain electrification towards emission control

As well as optimizing conventional drive concepts, motor vehicle manufacturers also rely on alternative concepts in order to ensure that existing and future noise and emission restrictions are complied with and reduce fuel consumption. The use of hybrid vehicles as a means of reducing environmental pollution and increasing driving pleasure and comfort is becoming increasingly popular. This is mainly driven by the tightening in pollutant emission standards and fuel economy regulations in the transport sector.

Hybrid vehicles are so defined because their propulsion systems are equipped with two energy sources, complementing each other: a high-capacity storage (typically a chemical fuel in liquid or gaseous form), and a lower capacity rechargeable energy storage system (RESS) that can serve as an energy storage buffer, but also as a means for recovering vehicle kinetic energy or to provide power assist. The RESS can be electrochemical (batteries or supercapacitors), hydraulic/pneumatic (accumulators) or mechanical (flywheel). This dual energy storage capability, in which the RESS permits bi-directional power flows, requires that at least two energy converters be present, at least one of which must also have the ability to allow for bi-directional powerflows [19].

The powertrain of a conventional vehicle is composed by an internal combustion engine, driving the wheels through a transmission that realizes a variable speed ratio between the engine speed and the wheel speed. A dry clutch or hydrodynamic torque converter interposed between engine and transmission decouples the engine from the wheels when needed, i.e., during the transients in which the transmission speed ratio is being modified. All the torque propelling the vehicle is produced by the engine or the mechanical brakes, and there is a univocal relation between the torque at the wheels and the torque developed by the engine (positive) or the brakes (negative).

Hybridization can attempt to address the following points [21]:

- *ICE efficiency improvement*: the secondary power source assists the ICE, preventing it from operating at inefficient conditions (e.g. at very high or very low engine speeds), i.e. operating the ICE nearer its best efficiency.
- *ICE downsizing/downspeeding*: due to the assistance of the secondary power source, a smaller ICE or a “longer” final drive can be chosen without compromising performance.
- *Power auxiliary/accessories electrically*
- *Higher control over the engine operating point and transients*: improved drivability and lower emissions
- *Eliminate or mitigate the clutch losses and (potentially) continuously varying gear ratio*
- *Regenerative braking*: When the vehicle is braking, its kinetic energy can be recovered by a generator and stored on-board.
- *Start and Stop enabled*
- *Idling reduction*: Depending on the sizing of the secondary power source, the engine can be turned off at stops and lower speed conditions

A possible classification of today’s vehicles in the market can be given based on internal combustion engine size and electric machine size as shown in Figure 1.1 and detailed in the following:

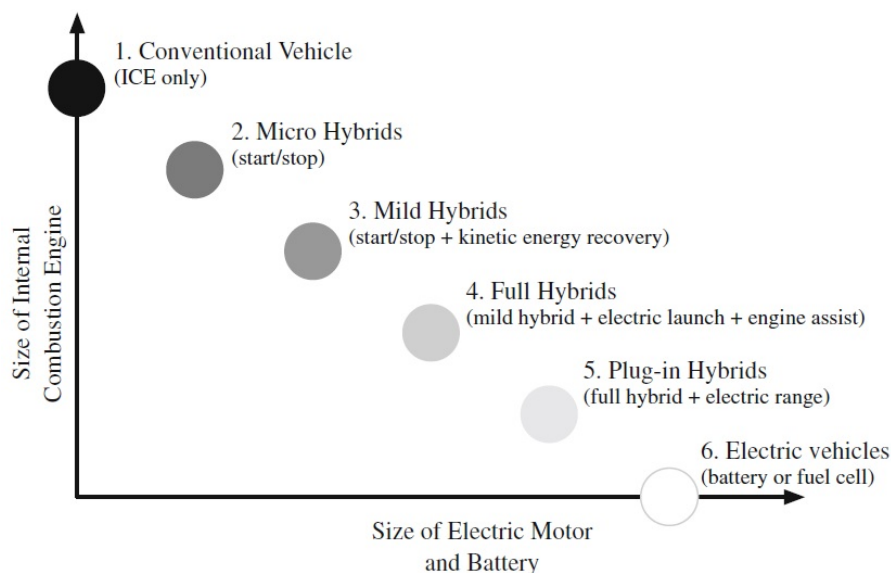


Figure 1.1: Hybrid electric vehicles classification [19]

1. *Conventional ICE vehicles*: in which the thermal power unit is the only source of power available to satisfy the power demand from the driver.
2. *Micro hybrids*: in which start and stop systems allows to switch-off and restart the ICE during idling, hence reducing fuel consumption and emissions.
3. *Mild hybrids*: here the ICE is coupled with an electric machine which is enabled to substitute the ICE while coasting or braking, enabling start and stop plus regenerative braking.
4. *Full hybrids*: which is the classification here adopted, can run in pure-electric, pure thermal or power-split operating mode. To coordinate such coupling, a proper Energy Management Strategy (EMS) is required to fully exploit the after-mentioned hybridization benefits.
5. *PHEVs*: are featured by the previous characteristics plus the ability to restore the battery charge by connecting the vehicle to an external power source.
6. *EVs*: under this category there are vehicles fully propelled by batteries (as PHEVs) or by hydrogen fuel cells.

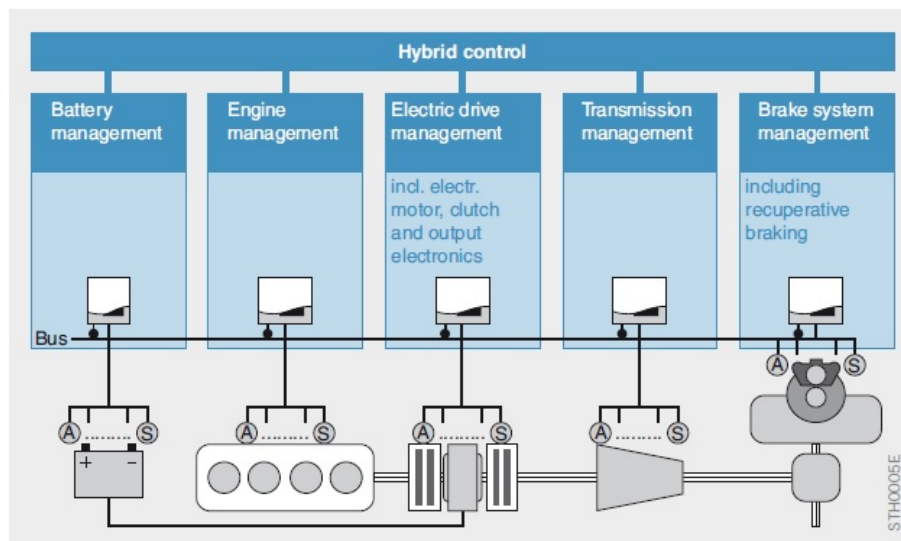


Figure 1.2: Networking of control systems in the drivetrain - A. Actuator B. Sensor [17]

Hence, HEVs EMS are characterized by complex logics (Figure 1.2) but allow most of the basic weaknesses of electric or internal combustion engine drive concepts to be reduced or even overcome. Despite these advantages, the market penetration of HEVs is still at its primal state since there are different alternatives in which the automotive manufacturers are actually involved in their research and development investments:

- Alternative fuels
- Alternative propulsion systems based on conventional frame
- Improvement in engine efficiency mainly driven to the obtain a cleaner combustion process

1.2 HEVs battery aspects in a growing circular economy

HEVs are also a key technology to decarbonise the road transport sector, but this is true until we consider their emissions from the on-board energy sources up to the tailpipe according to a so-called *Tank-to-Wheel Approach (TTW)*. At this point, by making reference to Figure 1.3¹, we have to underline that the effectiveness of the hybridization in terms of emissions is clearly affected by the amount of renewable energy sources adopted for the production of electric power, hydrogen and gaseous or liquid fuel to propel the vehicle and, particularly, on the distribution grid across the Countries. Nevertheless, there is still a certain awareness about the customer acceptance related to HEVs limited driving range, deployment or failure of batteries and their recharging structures, increase in vehicle weight, lack of smart grids to withstand with local peak current requests and maintenance cost.

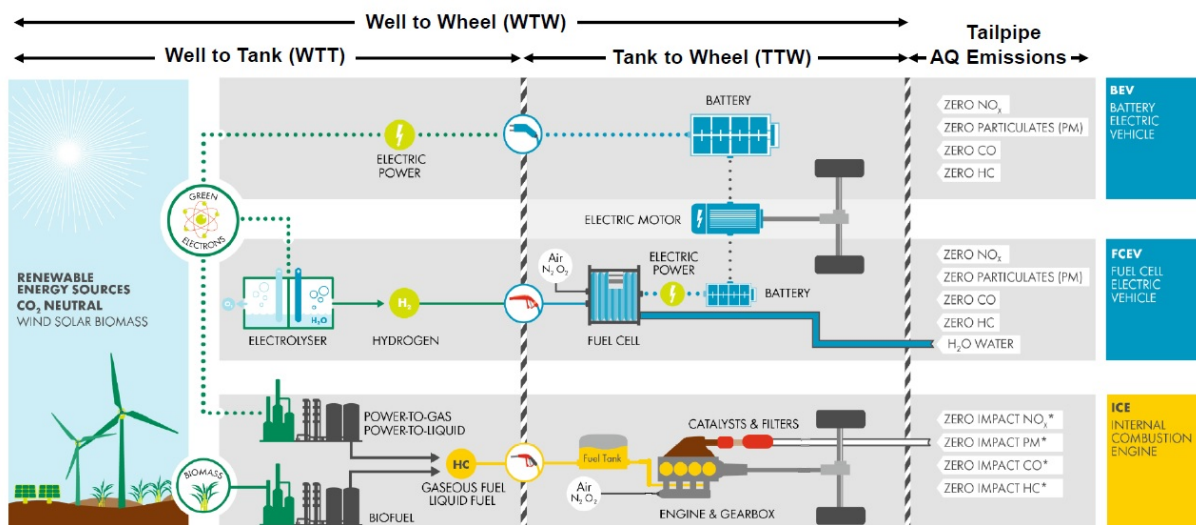


Figure 1.3: Roadmap for a zero impact mobility (*post Euro 6/VI)

This is enough to state that in the next decade a large number of vehicle manufactured will be run by internal combustion engines - 80% to 85% - with a growing rate of hybridization and improvements in terms of combustion and after-treatment efficiency. This statement has been deeply investigated and confirmed by most of the Original Equipment Manufacturers (OEMs) and international consulting groups, as depicted in Figure 1.4.

Moreover, one of the key-issue related to HEVs is the *battery ageing and value chain*. At present, lithium-ion batteries are the most common type of battery used in these vehicles; consequently, the projected diffusion of EVs is expected to increase demand for lithium-ion batteries. The question of what will happen to the huge number of lithium-ion batteries that reach the end of their life is important for the EU, which has set as a priority the development of a full value chain for batteries in Europe. How the valuable materials within each battery can be recovered and recycled will thus become more important, as will information on the impacts of developing a lithium-ion battery recycling industry within the EU.

¹The Road to Sustainable Fuels for Zero Emissions Mobility - Shell/OVK

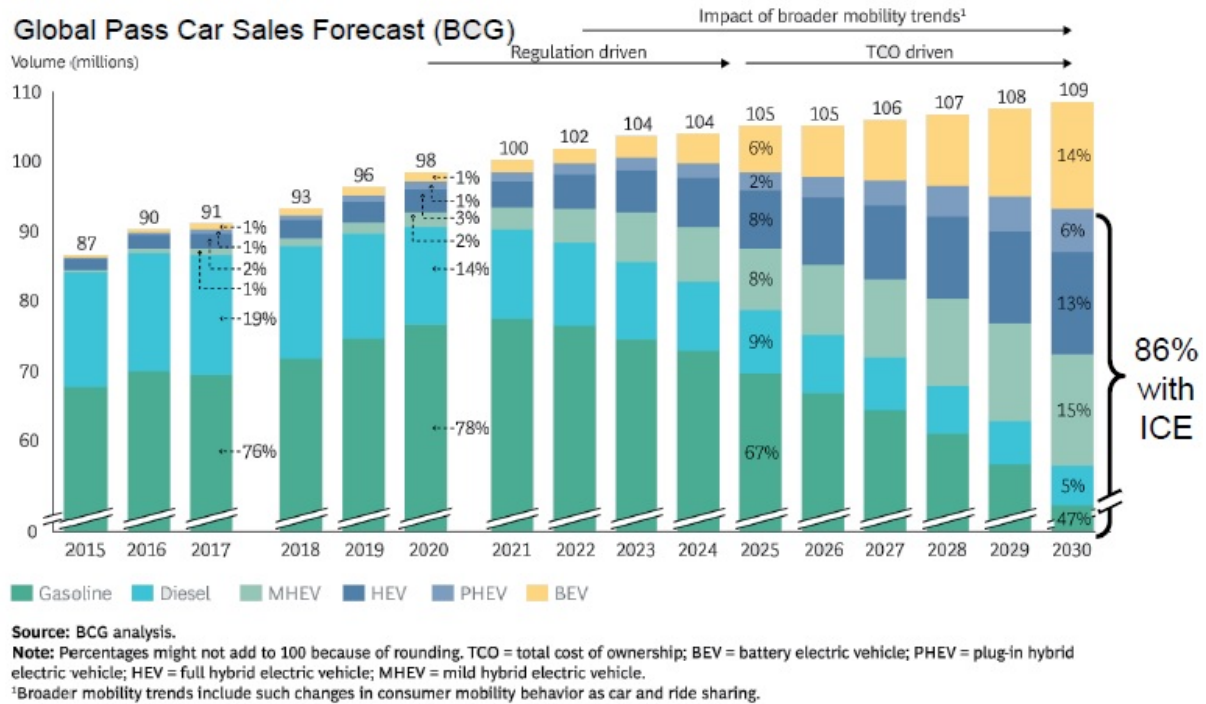


Figure 1.4: Global passenger car sales forecast - Source: Boston Consulting Group

In the paper [2] has been stated that increasing the collection and recycling efficiency rates of EV batteries in the EU can mitigate dependence on imported materials and help to retain the value of recovered materials in the EU economy.

- It is estimated that by 2030, €408 to €555 million in current prices could be recovered from the four key materials included in the study, i.e. cobalt, nickel, aluminium and lithium from EV batteries.
- In 2040, these figures could increase to around €1.9 billion to €2.6 billion
- Regarding cobalt, a critical raw material, 2,922 tonnes of material worth of €213 million could be recovered by 2030 up to 4,058 tonnes with a value of €295 million; this amount is 41% of all cobalt imports into the EU in 2012. In 2040, 18,763 tonnes of material worth around €1.37 billion could be recovered.
- The value of nickel that could be recovered in 2030 (€157 million) is around 9% of the value of net EU imports in the year 2015.
- Further potential benefits include job creation in the lithium-ion recycling sector for the collection, dismantling and recycling of EV batteries.
- The study also concludes that recycling certain materials in lithium-ion batteries, as opposed to extracting the raw material, may mitigate CO₂ emissions. The net savings of over 1 million tonnes of CO_{2,eq} in 2040 are equivalent to the CO₂ emissions of producing 261,000 tonnes of aluminium, which is comparable to the annual production of two primary aluminium smelters.

The lithium-ion battery value chain can be divided into six key segments (Figure 1.5), starting with the mining and processing of the raw materials right up until the recycling of the end product, with cell component, cell manufacturing, battery pack manufacturing and electric vehicle manufacturing between.

The extraction of minerals and raw materials used in lithium-ion batteries along with the processing of these materials generally takes place outside the EU. China is the leader in cell-component manufacturing and cell-manufacturing; in 2014, it had a 41% share of the global automotive cell manufacturing capacity, while the EU had a 5% share. The next stage of the process is battery-pack manufacturing, which accounts for approximately 40% of the cost of an EV battery. Regarding EV manufacturing, similar to the US and Japan, the EU has a global market share of 22% of the top 20 plug-in hybrid electric vehicles (PHEV) and battery electric vehicles (BEV) producers, while China is the leader with a 33% market share. As for the recycling of EV batteries, although the EU is in a strong position (mainly due to the legislative requirements in the field) it is not yet prepared to manage a large number of end-of-life batteries (*Lebedeva et al., 2016*). One part of the value chain that seems to be missing from Figure 1.5 is the option for second-life applications. This would typically appear between EV manufacturing and recycling, and should be considered when interpreting the value chain.



Figure 1.5: Automotive lithium-ion battery value chain

Chapter 2

HEVs Control Strategies Optimization

Hybrid Electric Vehicles (HEVs) offer improved fuel economy and lower emissions than conventional vehicles, mainly due to the possibility of engine downsizing, recovery of vehicle kinetic energy (regenerative braking) and power-split (thermal-to-electric) optimization. *Plug-in Hybrid Electric Vehicles (PHEVs)* might also take advantage of an external electrical charge - *grid* - leading to further fuel and pollutant reduction ¹

Despite any hybrid vehicle requires a control strategy, as far as enough energy is stored in the battery, PHEVs adopt a *charge-depleting* operation strategy: if the required traction power can be fulfilled by the electrical source, which is usually bigger and more performant than HEV, only the battery provides power until its almost total depletion ($SOC_{min} \cong 10 - 15\%$). Given that HEVs can uniquely run in *charge-sustaining mode* ($SOC_{min} \leq SOC \leq SOC_{max}$), a smart control strategy is required to fully exploit the potential of HEVs. In Figure 2.1 the two behaviour are easily depicted:

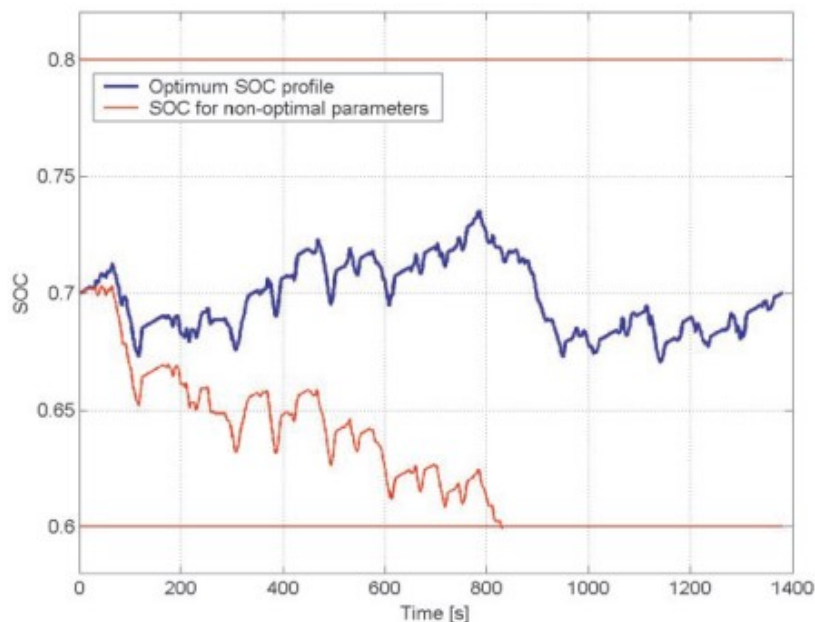


Figure 2.1: Charge-Sustaining vs. Charge-Depleting behaviour

¹The last condition is even more true if the grid is not powered by carbon-based fuel sources, and if we consider the tank-to-wheel emissions rather than well-to-wheel ones.

The *control strategy* consists in an algorithm that regulates the operation of the power-train and flashed into the *Engine Control Unit (ECU)*. Potentially, there is a large number of control strategies that can be applied on a given HEV architecture but the optimal one(s) depends on the target of the control strategy, e.g fuel consumption, battery SOC, operative costs, thermal management and classified according to the application and the on-board implementation attitude. Thus, the algorithm takes input data, e.g. the vehicle speed, the vehicle acceleration and the road grade, and makes decisions on the power demand from specific vehicle components.

Several HEV Battery Management Strategies (BMS) have been proposed in literature to identify the optimal control strategy. It follows that optimization methods can roughly be divided into two main categories and 4 subsets [21]:

- Not on-board implementable
 - *Global Optimization Methods* used for benchmark
 1. Dynamic Programming
 2. Genetic Algorithm
 3. Pontryagin's Minimum Principle
- On-board implementable
 - *Instantaneous Optimization Methods*
 1. Equivalent Consumption Minimization Strategy (ECMS)
 2. Adaptive - ECMS
 - *Heuristic Methods*
 1. Fuzzy Logics
 2. Rule-Based Methods
 3. Neural Networks
 - *Artificial Intelligence based Methods*
 1. Problem-Supervised Machine Learning
 2. Problem-Unsupervised Machine Learning
 3. Reinforcement Learning

For the sake of simplicity, a detailed overview of the computational methods adopted in the present work will be discussed in the following sections

2.1 Global Optimization Methods

Global optimization method are powerful tools to describe deterministic phenomena, i.e. for which a condition exists for each time step and boundary conditions are known a-priori, widely used as a benchmark stand in control application. For such methods, the optimality is given by finding the best path between the value of a given state s at time t and the value of its successor states at time $t+1$, hence finding the solution to the *Bellman equation* [3]:

$$v_{\pi}(s) = E_{\pi}[R_{t+1} + \gamma G_{t+1} | S_t = s] \quad (2.1)$$

where v is the value of an action at a given state s under the policy π ; E is the Expected value for the policy π ; S is the global set of states; γ is known as discount factor, usually closer to 1; R is the Reward, expressed as the rate of probability that a condition could exists or not at time $t+1$; G is the Expected Return, i.e. the sum of Rewards in the following time steps until the end of the mission.

Once the *policies* π (or F) - sets of control strategies - are defined, the one that optimize the objective function over the entire mission is chosen. The *optimal policy* π^* (or J) is derived by the following formulation:

$$\pi^*(s) = \min_{\pi(s) \in F(s)} J(\pi(s)) \quad (2.2)$$

Problem states are thus defined for each time step of the mission as

$$\pi^*(t) = \min_{\pi(t) \in F(t)} J(\pi(t)) \quad (2.3)$$

for which state-variable constraints (e.g. Battery SOC final value) are applied at each time step.

$$SOC_T = SOC_{t=0} \pm \epsilon \quad (2.4)$$

where ϵ is a small number used for creating a thin tolerance band. The SOC constraint is fundamental for having comparison between different HEV architectures and the conventional vehicle (regulation final SOC limitation).

2.1.1 Dynamic Programming

Dynamic Programming (DP) algorithm is an optimization technique widely adopted in the identification of the optimal control strategy in hybrid vehicles. The methodology was first introduced by Richard Bellman and Robert E. Kalaba in 1965 [3] and consists in finding the optimal solution - *optimality* - for specified sets of problem discretized on n-stages, i.e. a multi-stage decision-making process, which involves:

1. *A dynamic system*
2. *An objective function*
3. *Control and state grids*
4. *Control variables*: Action taken by the system (e.g. power-flows)
5. *State Variables*: System operating conditions (e.g. Battery SOC, ICE ON/OFF)

The last two items build the *computational grid* expressed as a multi-level combination of both. The grid is then formed by nodes.

The DP optimization algorithm consists of two phases [21]. The first phase is the *Backward phase* in which the cost function is evaluated considering all the combination of State of Charge and Engine States, i.e. the state variables at the end of the interval and all the combinations of control variables (PF and GN) found within. The fuel consumption in this interval is computed by reading from the configuration matrix the fuel consumption at the extreme of the interval and integrating them over the time interval. Also the engine state at the end of the interval is read and thanks to the battery model it is computed the SOC value and a score is assigned. The tool detects the best combination of control variable for all possible combinations of state variables. The procedure is iteratively repeated moving backwardly in the time grid, from the last to the first interval defining step-by-step the so called "*Cost-to-Go*" function, the "shortest route". At each backward step is fundamental to save the optimal function in order to follow the optimal path in the opposite direction during the following *Forward phase* once the overall backward procedure is over. Table 2.1 summarizes advantages and disadvantages of a dynamic programming controller, while Figure 2.2 represents an example of a DP computational grid.

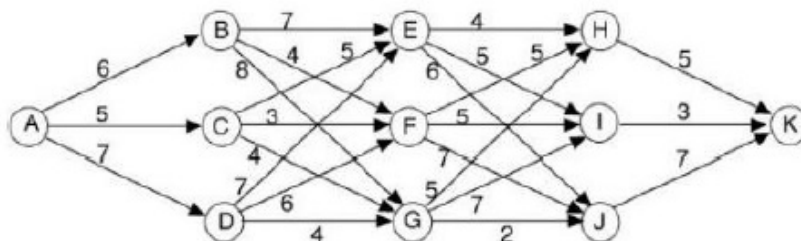


Figure 2.2: Dynamic Programming Computational Grid

Advantages	Disadvantages
<ul style="list-style-type: none"> - Complete control on non-differential non-linear problem - Wide application - Convergence to the optimal solution - Benchmarking 	<ul style="list-style-type: none"> - Mission to be know a-priori - Large constraints on discretization - Large memory requirements for storing intermediate steps - Not on-board implementable

Table 2.1: Dynamic Programming advantages and disadvantages

2.2 Instantaneous Optimization Methods

These methods involve the identification of an *Optimal Energy Management Strategy (Optimal EMS)* within the thermal and electrical power-unit output, based on the instantaneous minimization of a cost function for each time step of the mission. If the cost function is properly defined, the final result can be closer the global optimum derived by a DP controller and can be implemented on-board due to its low computational cost.

2.2.1 Equivalent Consumption Minimization Strategy - ECMS

ECMS consists in minimizing the cost function expressed as the sum of the internal combustion engine (*ICE*) fuel consumption and the energy conversion performed by the on-board energy sources, i.e. batteries and electric machines (*EM*), in terms of equivalent consumption through a suitable conversion factor. The latter must be tuned according to the mission in order to reach the optimality and it is known as *Equivalence Factor (EF)*. *ECMS Cost Function* is thus expressed as:

$$J_t = \dot{m}_{ICE}(P_{ICE}(t)) + \zeta(P_{EM}(t)) \quad (2.5)$$

In literature there is a wide range of ECMS formulation; the commonest one was introduced in 2005 by *Musardo et al.* [4], which expresses the equivalent fuel consumption of the EM as:

$$\begin{aligned} \zeta(P_{EM}(t)) = \gamma \cdot s_{dis} \cdot \frac{1}{\eta_{batt}(P_{EM})\eta_{EM}(P_{EM})} \cdot \frac{P_{EM}(t)}{H_i} + \\ (1 - \gamma) \cdot s_{chg} \cdot \eta_{batt}(P_{EM}) \cdot \eta_{EM}(P_{EM}) \cdot \frac{P_{EM}(t)}{H_i}; \\ \gamma = \frac{1 + \text{sign}(P_{EM}(t))}{2} \end{aligned} \quad (2.6)$$

where η_{batt} and η_{EM} are the battery and the electric machine efficiencies as a function of the actual mechanical power $P_{EM}(t)$ drawn by the electric machine, respectively, while H_i is the lower heating value. s_{chg} and s_{dis} represent the Equivalence Factors (EFs) and they are the *control parameters* of the ECMS approach, kept constant during the whole mission and cycle dependent.

The last statement is a key-point, since one of the drawbacks of this algorithm implies that an optimal solution is obtained if the cycle is known a-priori. $P_{EM}(t) > 0$ in traction for convention, so that:

- $\gamma = 1$ i.e., $P_{EM}(t) > 0$ the equivalent consumption is related to the electric motor only running in a pure electric mode
- $\gamma = 0$ i.e., $P_{EM}(t) < 0$ the equivalent consumption is related to the ICE-side and provides energy to increase the battery State of Charge (SOC) of the EM which works as a generator i.e., vehicle running in Battery-Charging mode
- $P_{EM}(t) = 0$ the equivalent consumption is null, and the vehicle operates in a pure thermal mode
- Otherwise, the vehicle would run in Power-Split mode in which the EM acts as a motor providing additional traction power to assist the ICE towards a higher efficiency operating point

The traction efficiencies are at the denominator in order to get a positive value, given that the onboard powertrains must hold a power to overcome losses and vehicle resistances and satisfy the driver requests. The optimal criterion for each time step and the relative boundary conditions (BCs) follow:

$$\begin{cases} [P_{ICE}^{opt}(t), P_{EM}^{opt}(t)] = \arg \min_{P_{ICE}(t), P_{EM}(t)} J_t & \text{if } P_{req} \geq 0 \\ [P_{ICE}^{opt}(t) = 0, P_{EM}^{opt}(t) = P_{req}] & \text{if } P_{req} < 0 \end{cases} \quad (2.7)$$

$$\begin{cases} P_{req}(t) = P_{ICE}(t) + P_{EM}(t) \\ SOC_{min} \leq SOC(t) \leq SOC_{max} \\ 0 \leq P_{ICE}(t) \leq P_{ICE,max} \\ P_{EM,min}(t) \leq P_{EM}(t) \leq P_{EM,max} \end{cases} \quad (2.8)$$

Apart the common formulation, a correlation at battery terminals is introduced with the aim of reducing the control parameters needed for calibration:

$$J_t = \dot{m}_{ICE}(P_{ICE}(t)) + \zeta(\eta \cdot P_{batt}(t)) \quad (2.9)$$

The battery power P_{batt} appearing in the formula indicates the net electrical power as seen at the battery terminals, which differs from the electrochemical power P_{chem} i.e., the power correlated to the effective SOC variation. If one assumes that the relation between this quantity and the electrical power can be represented as a battery charge/discharge efficiency η_{batt} , then:

$$\begin{cases} s_{chg}(t) = \lambda(t) \cdot \eta_{batt} & \text{while charging} \\ s_{dis}(t) = \frac{\lambda(t)}{\eta_{batt}} & \text{while discharging} \end{cases} \text{ yields to} \quad (2.10)$$

$$s_{chg}(t) = \eta_{batt}^2 \cdot s_{dis}(t) \quad (2.11)$$

Moreover, a SOC penalty function has been introduced [19] to guarantee the charge-sustainability of the algorithm and to fix the SOC within the admissible range defined by the upper and lower SOC value. The penalty function plays a critical role to achieve a reliable online estimation of the battery SOC and its deviations from the target value. Thus:

$$p(SOC) = 1 - \left(\frac{SOC(t) - SOC_0}{0.5 \cdot (SOC_{max} - SOC_{min})} \right)^a \quad \text{with a odd number } a \in \mathbb{N} \quad (2.12)$$

so that the ECMS objective function 2.5 can be modified by multiplying the equivalent consumption by the penalty function 2.12 as:

$$J_t = \dot{m}_{ICE}(P_{ICE}(t)) + \zeta(P_{EM}(t)) \cdot p(SOC) \quad (2.13)$$

- if $p(SOC) < 1$ a lower cost is attributed to the battery energy, thus making the discharge more likely when the SOC is above the reference value.
- if $p(SOC) > 1$ a higher cost is attributed to the battery energy to make its discharge less likely.

Those statements are summarized in Figure 2.3. Equation 2.5 has been used as the objective function of the present work.

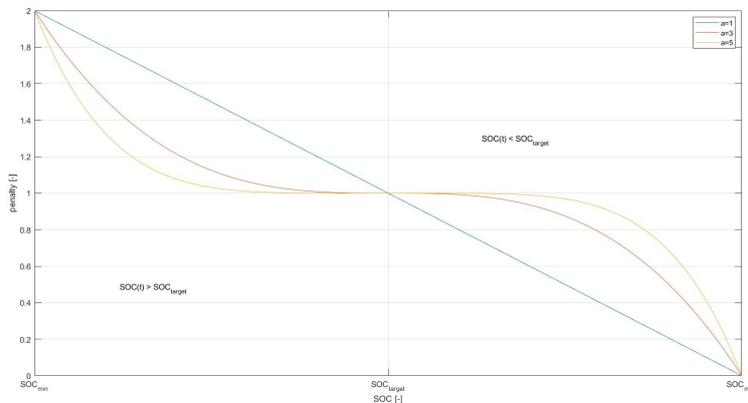


Figure 2.3: SOC penalty function

2.2.2 Adaptive - ECMS

ECMS Algorithm has several drawbacks:

- *Constant EFs*: The algorithm cannot adapt to unpredicted variations in control and state variables following different driving patterns or stochastic phenomena. The design parameters i.e., the Equivalence Factor, are kept constant during the whole mission
- *Driving Cycle*: Even if a proper calibration is made up for a certain layout, the EFs are cycle dependent and a given pair cannot be used for different traffic scenarios. This implies that the driving cycle must be known a-priori but this condition, which is not deterministic, cannot be always satisfied even if we have a sophisticated Global Positioning System
- *Computational Cost*: Despite the lower time required for solution with respect to DP, ECMS requires a high level of hardware to be executed online

A solution to overcome the uncertainty and the lack of flexibility coming from ECMS in defining the EFs is driven by the *Adaptive - ECMS (A-ECMS)*, which adapts the EFs as a function of a feedback obtained from vehicle components such as batteries, tachometer, torque control or after-treatment system. Thus EFs can be instantaneously or periodically updated, making the algorithm *adaptable* to stochastic phenomena and more prone to be executed online with modern ECU.

In literature several adaptive formulations have been proposed. For the easiness of consultation we can resort them in the following categories, listed in growing order of implementation complexity:

- EFs adaptation based on SOC feedback from batteries [4], [5], [6], [19]
- Casual set-theoretic method for online EFs estimation [7]
- EFs adaptation based on speed prediction [8] [9]
- EFs adaptation based on driving style recognition [10], [11]
- EFs adaptation based on actual pollutant emissions [12]
- EFs adaptation based on torque control [13]
- EFs adaptation based on Intelligent Transportation System [14], [15], [16]

The present work will discuss the implementation of three different control strategies with the aim of identifying and proposing the proper algorithm for the study case under investigation. In particular:

1. Instantaneous (or continuous) A-ECMS

- EFs adaptation based on the instantaneous SOC feedback
- The algorithm initialization is based on EFs obtained from the Design of Experiment Approach
- Highest computational time with respect to other approaches

2. Discrete (or periodic) A-ECMS [19]

- EFs adaptation based on periodic SOC feedback and tuning performed by a proportional derivative controller
- Requires high level of calibration
- Lower computational time with respect to the instantaneous approach

3. Hybrid A-ECMS

- It is a brand-new controller proposed after a deep understanding of the controller and its literature
- EFs adaptation is based on a periodic update as a function of the SOC feedback and a PI controller, with similar characteristics compared to the discrete approach, plus an instantaneous correction based on vehicle speed and acceleration
- Implies a computational time in the average between the previous strategies and the highest level of calibration

Chapter 3

Model

The present work takes advantage of a pre-existing tool developed for layout and control strategy optimization of HEVs called *HEVBox* [25]. Such optimization tool runs on Matlab and it is used for HEVs Research and Development purposes. Its workflow can be summarized as follows:

1. *Model Input*: the user defines the HEV architecture and characteristics (vehicle setup and powertrain data), the driving cycle and a powerflow strategy
2. *Data Processing*: the main kernel of this optimization tool implies a *pre-processing phase* - during which the vehicle virtualization and the time grid are performed based on the model input - and a following one in which the feasible outputs obtained from the pre-processing phase are used to compute the objective function and state the optimal policy of the driving mission, called *optimization phase*.
3. *Post Processing*: Several scripts are available to report and analyse the solutions obtained

In the following section, a detailed overview of these steps will be presented.

3.1 Model Input

3.1.1 Architecture Definition

The optimization tool defines *architecture* the following dataset:

- Engine displacement [l]
- Electric machine peak power [kW]
- Power-to-Energy (PE) Ratio [W/Wh] ¹
- Electric machine coupling speed ratio with the main shaft
- Final drive speed ratio
- $Crate_{max,dis}$
- $Crate_{max,chg}$
- Charging equivalence factor coefficient s_{chg}
- Discharging equivalence factor coefficient s_{dis}

The C-rate is a measure of the rate at which a battery is being discharged. It is defined as the discharge current divided by the theoretical current draw under which the battery would deliver its nominal rated capacity in one hour. A 1C discharge rate would deliver the battery's rated capacity in 1 hour. A 2C discharge rate means it will discharge twice as fast (30 minutes). Battery packs with higher PE ratios, have less storage capacity [Wh] over which to distribute peak power demand [W], and hence require thinner electrodes to deliver higher power. Thinner electrode cells, while enabling higher power outputs, are more expensive on a per kWh basis due to higher costs associated with the inactive materials, such as separators and current collectors.

As reported in the abstract, a p2 parallel hybrid configuration has been used to assess the transformation of a conventional heavy-duty vehicle featured by a 4.5L diesel engine into a full hybrid version.

The expression *parallel hybrid drive* (Figure 3.1 [17]) is used to describe an arrangement of hybrid components in which the electric motor and the internal-combustion engine can both individually deliver their output to the drive. If necessary, the outputs can be combined by means of mechanically coupling the motor and the engine to the drive. The possibility of power addition allows the machines to be made with relatively small dimensions without adversely affecting the driving performance. The components that are required are designed according to the most frequent area of use.

There are different types of implementation. The electric motor can be directly flanged to the crankshaft (crankshaft-mounted starter-alternator) or coupled to the internal combustion engine by a belt drive. Both drive sources can be used together or individually to propel the vehicle. Since only one electric motor is incorporated in the system, the vehicle cannot be electrically powered while the battery is being charged.

¹Source: <http://energy.mit.edu/news/whats-cost-got-to-do-with-it/>

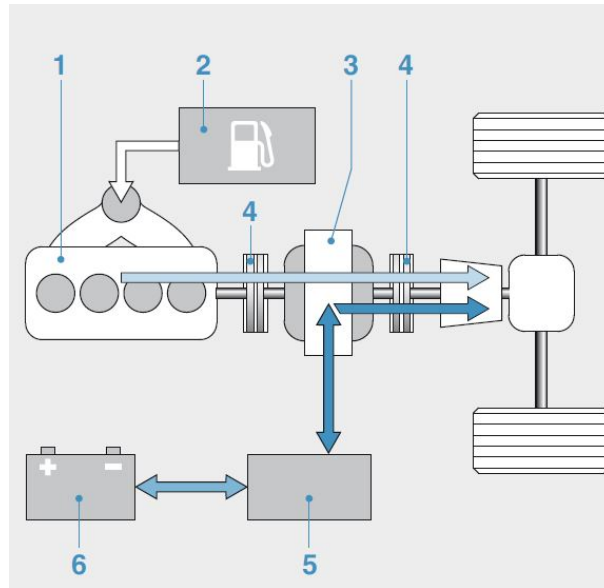


Figure 3.1: Parallel Hybrid configuration

1. Internal Combustion Engine; 2. Fuel Tank; 3. Electric Motor/Alternator;
4. Coupling devices; 5. Inverter; 6. Battery

The electric motor can only operate as an alternator or for drive purposes. If a coupling is integrated between the electric motor and the internal-combustion engine (Figure 3.2²), the engine does not have to be carried along when the vehicle is being propelled using purely electric power. Such arrangement is known as *p2 single-shaft parallel hybrid* architecture in which the electric motor is mounted between the engine and the transmission unit, with the capability to decouple it from the engine through a specific clutch. The power flows from the battery to the electric motor through an inverter and a torque coupling device provides the connection to the ICE. All the power is transferred to the front axle.

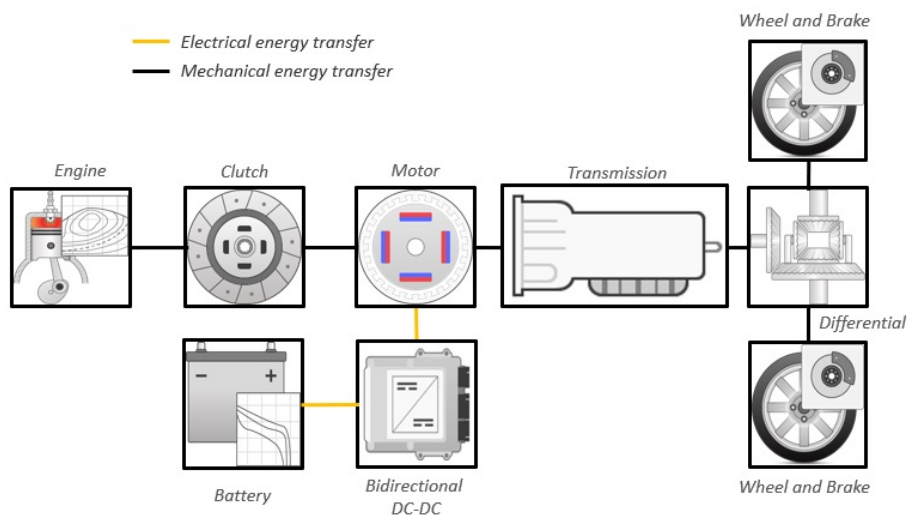


Figure 3.2: P2 Parallel Hybrid configuration

²Source: Mathworks

Hence, given the mechanical coupling between the engine and the driven wheels, the control of the parallel hybrid drivetrain is more complex but the major advantages of a parallel configuration with respect to a series configuration are:

- A generator to transform the mechanical power coming from the thermal unit into electrical power to sum up to the power coming from the batteries is not required
- The traction motor is smaller
- Multiple power conversion are not required - higher driveline efficiency
- Drag torque losses can therefore be avoided

These advantages lead the larger diffusion of the parallel configuration with respect to the series one; in the present work a p2 configuration, perhaps, has been introduced.

Powerflow Strategy

Hybrid architectures can satisfy driver's power request by using the thermal power unit and electrical machines exclusively or in conjunction. The way in which this happens is defined by the powerflow - from now on *PF*. In HEVbox, four powerflow categories are defined:

1. *Pure Electric (PE)*: the electric motor alone provides the power required to move the vehicle and the engine is off. Regenerative braking is included in this category.
2. *Pure Thermal (PT)*: the engine alone provides the power required to move the vehicle and the electric machines are off. Electrical power drawn from ICE auxiliaries are also accounted for in the battery SOC variation during this operating mode.
3. *Power Split (PS)*: both the engine and electric machine(s) provide power to propel the vehicle.
4. *Battery Charging (BC)*: the engine is on and the electric machine acts as a generator. The engine provides more than the power required to move the vehicle; the excess power is converted into electrical energy by the electric machine and stored into the battery. It is assumed that this operating mode is only allowed when the vehicle is in motion.

The operating mode (Figure 3.3) is defined by the *gearbox gear number* (GN) and the powerflow (PF), which represent the *control variables* of the simulation environment. Based on the vehicle operating conditions, there may be some restrictions on the powerflow that can be selected by the control strategy optimization algorithm. These restrictions always apply to individual time-steps. In particular, the vehicle is forced to stay in pure electric mode when braking, which means that regenerative braking is always performed when possible. Moreover, is also forced to stay in pure electric mode when it is at stand-still. For architectures featuring a single electrical machine on the primary axle, the powerflow can be identified by a unique parameter that defines the share of the power demand provided by the electric machine, expressed as:

$$\alpha = \frac{P_{EM,p}}{P_{req}} \quad [-] \quad (3.1)$$

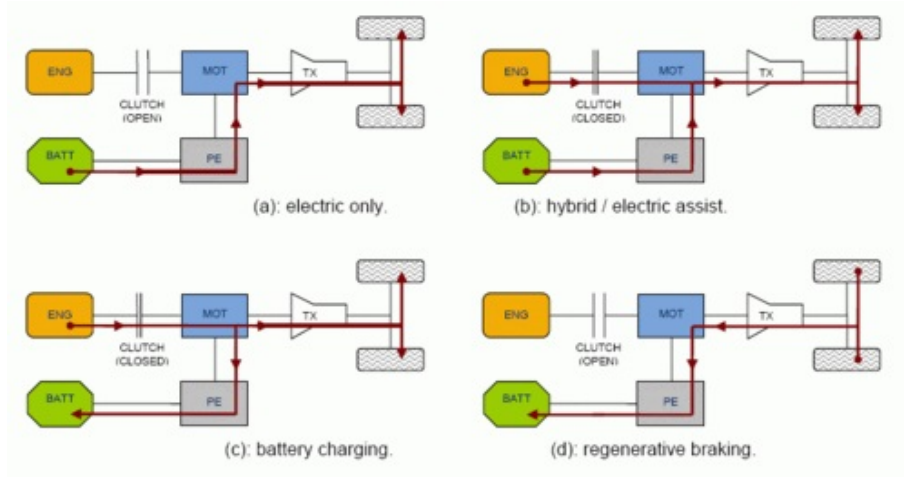


Figure 3.3: Hybrid Operating Modes

where $P_{EM,p}$ is the power provided by the electric machine (or absorbed, if negative) and P_{req} is the power required for motion. p2 architecture powerflow strategy is hereby reported in Table 3.1:

p2 powerflow	PU involved	α
PE	EM	1
PT	ICE	0
PS	ICE+EM	0.25; 0.5; 0.75
BC	ICE+EM	-0.5; -1; -1.5

Table 3.1: p2 architecture powerflow strategy

3.1.2 Electric machine

The electric machine adopted is of the brushless permanent magnet type, that can work either as a generator and as a motor. Such electric motors are commonly adopted in hybrid vehicles given their high efficiency, compactness, easiness in maintenance and control plus a high energy density. The electric propulsion system, thus is made up of three main components:

- *Electric machine*: can propell the vehicle (PE,PS) or recharge the battery (BC)
- *Power converters*
- *Electronic controllers*

3.1.3 Battery pack and electrical energy accumulators

Lithium-ion batteries have been adopted in this study as the secondary power storage device. Irrespective of the design of the hybrid vehicle (serial, parallel or split-power hybrid), the vehicle electrical system consists of at least two subsystems with different voltage conditions:

- The traction power supply for supplying the electrical part of the drivetrain; the nominal voltage is significantly above 42 V in this case, whereby the battery voltage can be less than the traction power supply voltage
- The conventional 12 V vehicle electrical system for supplying the body components (power windows, radio etc..) and the internal-combustion engine (engine control unit, radiator fan, additional water pump etc.)
- A sub-power supply with different voltage conditions if necessary

Both the traction part and the body part of the vehicle electrical system are equipped with an energy accumulator. A facility for connecting the voltage levels using a DC/DC converter is usually provided. The provision of a power supply network with different voltage conditions and the way in which it is connected to the other sub-power supplies depends on the design of the respective hybrid vehicle. In order to ensure that the battery operates reliably with a high voltage condition in a hybrid vehicle, a control unit (battery management system) is needed that monitors the individual battery components and controls charging and discharging, thermal management and various safety functions.

SOC: State of Charge

The energy accumulator is operated at an average charge level in order to achieve good recuperation current absorption and good power output in order to assist acceleration. High charge levels provide high power output, and low charge levels make it possible to feed back large quantities of recuperated electrical energy. The SOC can be computed as:

$$SOC_t = SOC_{t-1} - \int \frac{I_{batt}}{C_{batt}} dt \quad (3.2)$$

The limit thresholds of the SOC are imposed to be [0.4-0.8]; the battery life is assumed to be 150000 Ah and the maximum current transferable through a cell is 120 A.

Energy accumulator for Heavy-Duty Hybrid Systems

Nickel metal hydride batteries (NiMH) have been used in the last decade as standard for hybrid vehicles. Nickel cadmium batteries are not used in modern vehicles given the toxicity and the environmental harm. Lithium battery systems are undergoing further development for use in hybrid vehicles. Compared to NiMH systems, lithium systems provide even higher energy and power densities at cell voltages of approximately 3.6 V, high energy efficiency and long life. These systems are therefore mainly used in portable electrical systems (mobile phones, laptops), where they have essentially replaced NiMH batteries. Efforts are currently being made to subject these cells to further development for use in hybrid vehicles. Special attention is being paid to the use of low-cost and reliable electrode materials (e.g. $LiMn_2O_4$, $LiFePO_4$).

The use of lightweight Li metal and the properties of the other materials involved (graphite as the anode material) make it possible to manufacture extremely thin electrodes (≤ 0.5 mm), which can be used to create structures with extremely high output (e.g. 3 kW/kg with SOC 60 %, 25 °C and 10 s pulse duration).

Because of the high energy content of the electrode material and the high cell voltage, special measures are required:

- Use of organic electrolyte with special conductive minerals
- Safety structures that prevent the cell from exploding if it becomes damaged
- Monitoring of individual cells in order to avoid overcharging and overheating

The positive electrode consists of special metal oxides (Ni, Mn, Co or mixtures) that can store lithium ions. These ions can move to the counter-electrode and back during the discharging/charging process in a reversible mechanism. During the discharge phase the lithium ions migrate from the negative electrode to the positive one through the electrolyte, while during the charge phase the process is reversed. The counter-electrode is made from graphite and can also absorb Li ions because of its stratified structure. The electrolyte is a liquid solution of dissociable lithium salt and an organic solvent.

Heavy-Duty vehicles have a considerable number of additional electrical consumers such as a lift platform, radio equipment, a television or a coffee machine. The dry-charged (i.e. the battery is ready for use after filling with electrolyte) heavy duty battery (HD battery) is maintenance-free in accordance with European Standard EN and includes a combination of measures for making the battery deep-cycle resistant and vibration-proof. It ensures a reliable power supply even under conditions of high continuous loading caused by a large number of electrical consumers. This type of battery is installed in commercial vehicles which are subject to high levels of vibration and cyclical loading. The HD-Extra battery features even more far-ranging characteristics. These are needed in order to withstand unusually high levels of loading:

- Extreme cold-start reliability (up to 20 % higher starting reserve)
- Extremely long service life
- Extremely vibration-proof (100 % more than EN)
- Extremely deep-cycle resistant (four times greater than standard batteries)

3.1.4 Internal Combustion Engine

Eurocargo truck family is powered by a turbocharged in-line 4 cylinder 4 strokes Diesel internal combustion engine with an air-to-air intercooler. The one adopted in the present work belongs to the Tector 5 engine series (Figure 3.4) designed by FPT Industrial SpA, a branch of CNH Industrial N.V. which provides the propulsion system for the whole segments of CNHi, including Iveco, Magirus, Magelys, etc.

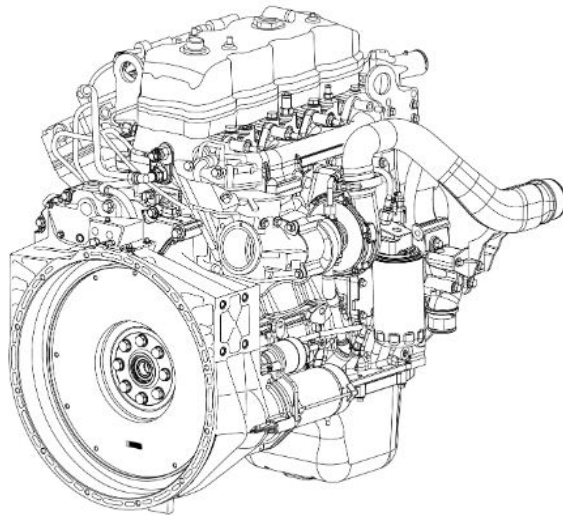


Figure 3.4: Tector 5 engine series - Source: Iveco SpA workshop manual

The engine fuel system is electronically controlled and the fuel is directly injected in the combustion chamber through a high pressure feeding pump and the common rail system, right before the combustion and is ignited by the elevated temperature of the air with high expansion ratio and lean air/fuel mixture. Intake and exhaust valve are actuated by the camshaft via a rocker system. The engine lubrication is obtained through a geared pump moved by the crankshaft, while a heater exchanger tunes the lubricant temperature. In a hybrid vehicle the thermal unit is assisted by the electric machine in order to be used more efficiently with respect to a conventional driveline, running at high power for longer period of times. The engine performances are modelled using look-up tables derived from experimental design. The mass flow rate related to the fuel consumption is expressed as a function of the mechanical engine power $P_{ICE,mech}$ and speed ω_{ICE} and recalled by a 2D interpolation map, while the corresponding CO₂ emission is linearly determined as:

$$\dot{m}_{CO_2} = 2,65 \cdot \frac{\dot{m}_{FC}}{\rho} \quad (3.3)$$

3.1.5 Auxiliaries

Auxiliaries are accounted by means of a constant power demand related to a plausible mean required power level, which is not hardcoded. They account for either electrical auxiliaries, i.e. power drawn from battery, and ICE auxiliaries, only considered when the engine is running.

3.1.6 Equivalence Factor definition by means of the Model-Based calibration

As seen in section 2.2.1 the main design parameters of the Adaptive-ECMS algorithm are the so-called Equivalence Factor, which represent the weight of the instantaneous equivalent consumption generated by the electric machine, either in charge and in discharge, over the objective function. One of the main issue regarding these factors is driven by correctly defying their numerical value, since the final result of the mission would differ even varying the third decimal value. To increase the chance of deriving the best set of initialization factor for each layout tested, a sampling method based on *Sobol sequences* has been introduced.

The *Model-Based calibration toolbox* [26] in Matlab uses the approach of the Design of Experiment (DoE) to generate a set of virtual test-benches to be modelled according to the declared input parameters. This is a mathematical and visual method of addressing problems of calibration and control of complex systems such as engines. Engineers can locate and correct errors early in system design when the time and financial impact of system modification are minimized. To perform this task, several algorithm are available. The one adopted in this work is the after-mentioned Sobol Sequence which belongs to the family of quasi-random sequences which are designed to generate samples of multiple parameters as uniformly as possible over the multi-dimensional parameter space (*Saltelli et al., 2010*).

One criterion for assessing the performance of a good sampling method is the discrepancy in the exploration of the multi-dimensional parameter space. The discrepancy metric was defined by Ilya M. Sobol and is the maximum deviation between the theoretical density $d_t = 1/N$ and the point density d_i in an arbitrary hyper-parallelepiped within the parameter space - hypercube (*Saltelli et al., 2010*). The sampling based on Sobol sequences is designed to generate samples with low discrepancy.

Figure 3.5 [27] shows that the points produced by a sampling based on Sobol sequences are more evenly distributed than the points produced with the other sampling techniques. As a result, the discrepancy in the exploration of the multi-dimensional parameter space is lower compared to the other sampling techniques.

The biggest difference with respect to pseudo-random numbers is that the sample values are chosen under consideration of the previously sampled points and thus avoiding the occurrence of clusters and gaps, this is the reason why such sequence has been chosen for the generation of the EFs dataset, by means of the *Space-Filling Design*.

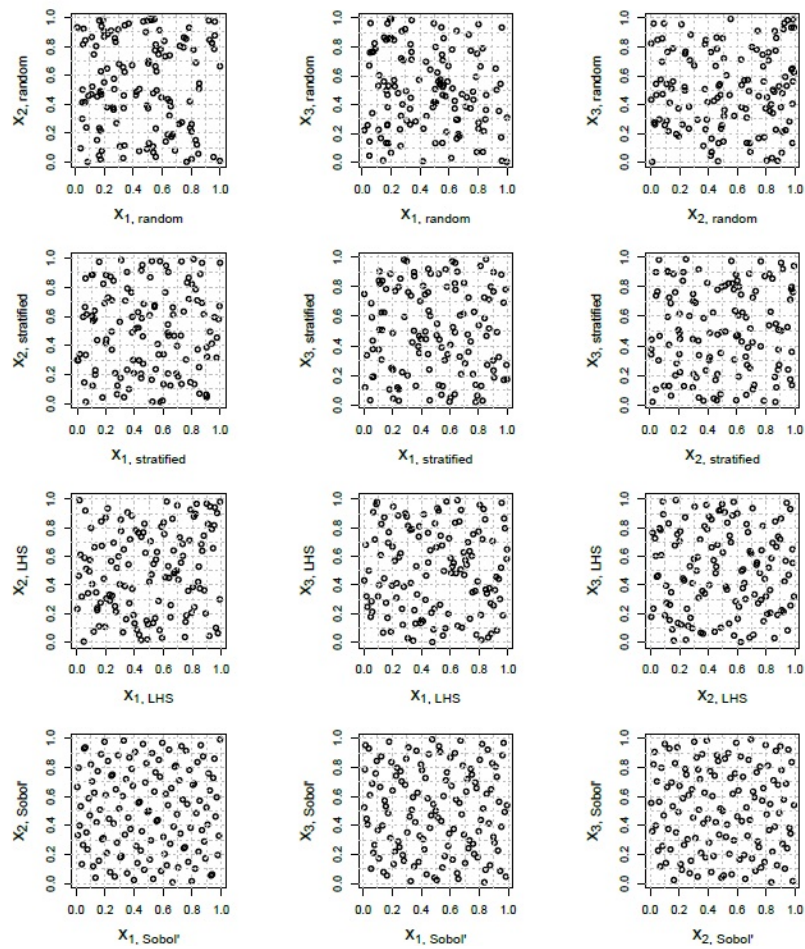


Figure 3.5: Top to bottom: Pseudo-random, stratified sampling, Latin hypercube sampling and sampling based on Sobol sequences

3.1.7 Driving Cycle

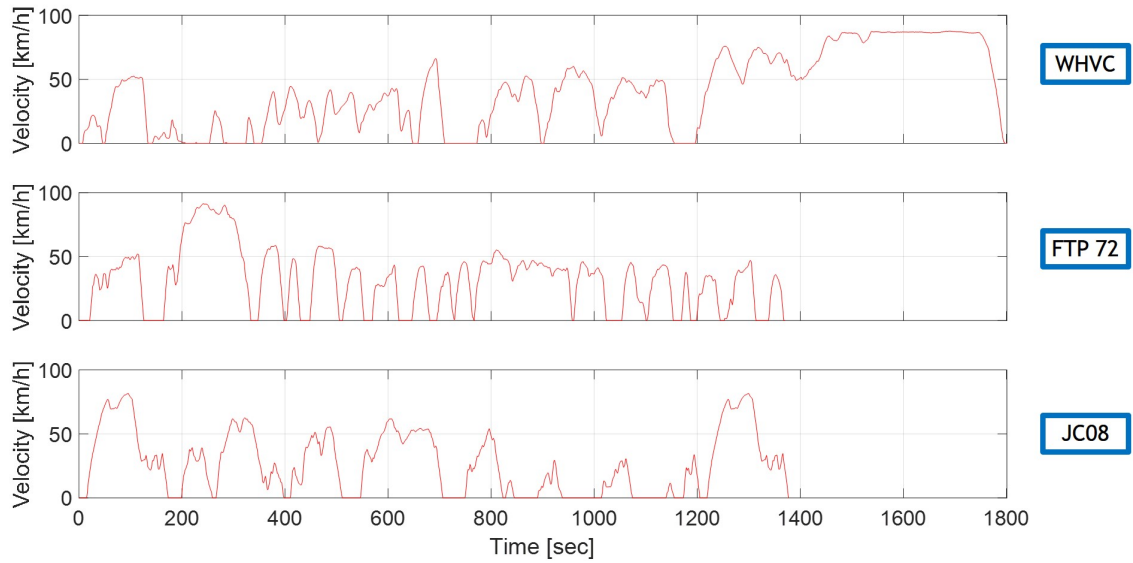


Figure 3.6: Driving Cycle

Figure 3.6 highlights the chosen driving cycle for the testing campaign, which will be analysed in the following to state their choice and their utility for the present work.

WHVC

The World Harmonized Vehicle Cycle (WHVC) is a chassis dynamometer test developed based on the same set of data used for the development of the World Harmonized Transient Cycle (WHTC). While the WHVC chassis dynamometer test is not identical to the WHTC engine test, the WHVC results have been occasionally used to compare the respective vehicle and engine emission levels for research purposes.

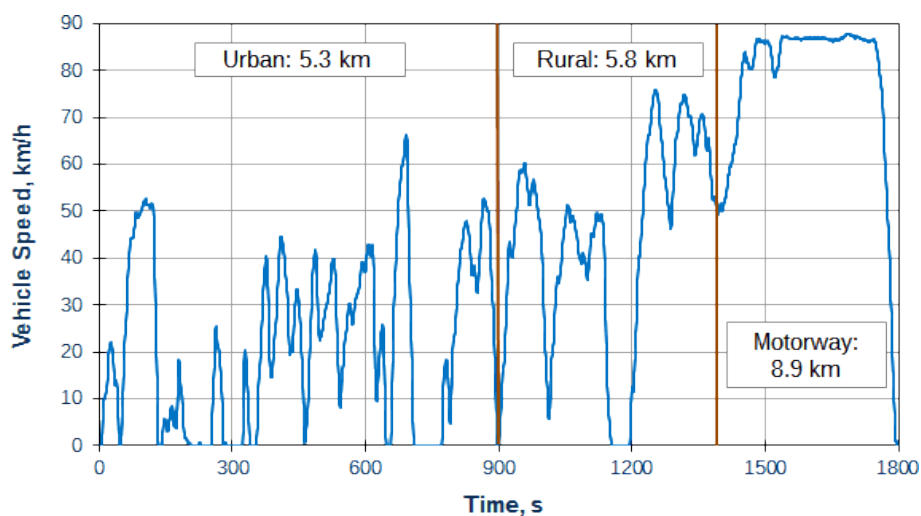


Figure 3.7: World Harmonized Vehicle Cycle (WHVC)

The duration of the WHVC test is 1800 s. The test includes three segments, representing urban, rural and motorway driving. With reference to Figure 3.7:

1. The first 900 seconds represent urban driving with an average speed of 21.3 km/h and a maximum speed of 66.2 km/h. This segment includes frequent starts, stops and idling. Weighting factor: 0.50
2. The following 481 seconds represent rural driving with an average speed of 43.6 km/h and a maximum speed of 75.9 km/h. Weighting factor: 0.27
3. The last 419 seconds are defined as highway driving with average speed of 76.7 km/h and a maximum speed of 87.8 km/h. Weighting factor: 0.23

The weighting applied each of the three segments can be varied between 0 and 1 to represent different classes of vehicle operation. The sum of the three weighting factors has to be 1.0.

FTP-72

The US FTP-72 (Federal Test Procedure) cycle is also called Urban Dynamometer Driving Schedule (UDDS). The cycle simulates a urban route of 7.5 mi (12.07 km) with frequent stops. The maximum speed is 56.7 mph (91.25 km/h) and the average speed is 19.6 mph (31.5 km/h). It is representative of a mixed driving cycle, which is the most frequently performed by the vehicle category under analysis.

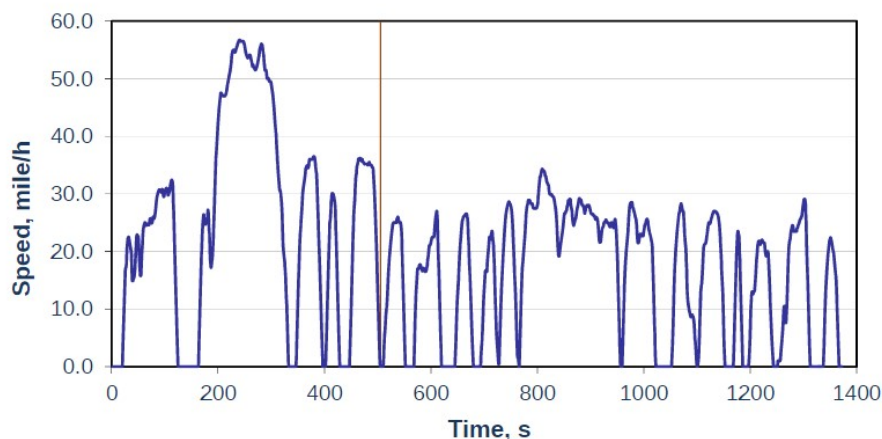


Figure 3.8: Federal Test Procedure - 72

It consists of two phases:

1. 505 s - 5.78 km at an average speed of 41.2 km/h with a cold start - Weighting factor: 0.43
2. 867 s - 6.29 km at an average speed of 28.7 km/h - Weighting factor: 0.57

JC08

The test represents driving in congested Japanese city traffic (urban test cycle), including idling periods and frequently alternating acceleration and deceleration. Measurement is made twice, with a cold start and with a warm start. The test is used for emission measurement and fuel economy determination, for gasoline and diesel vehicles. It is part of a wider test procedure which is the JE05 transient test cycle based on Tokyo driving conditions, applicable to diesel and gasoline vehicles.

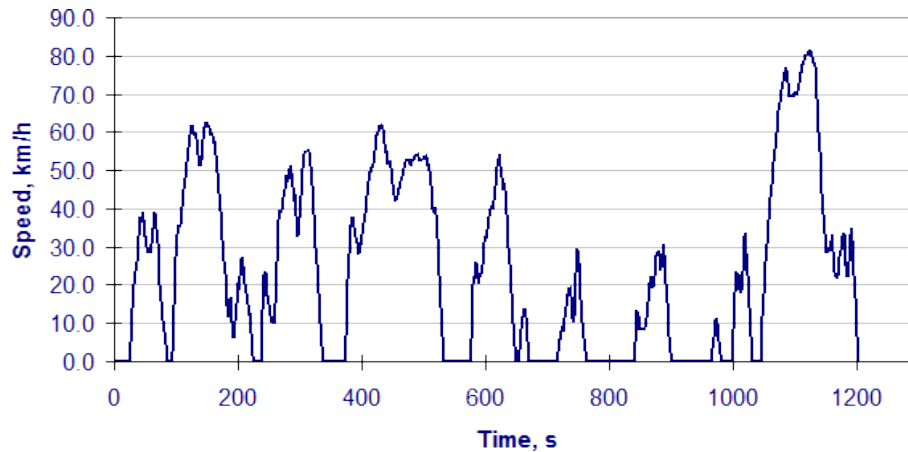


Figure 3.9: Japan Cycle 08

The JC08 test had been fully phased-in by October 2011, with the following features:

- Duration: 1204 s
- Total distance: 8.171 km
- Average speed: 24.4 km/h (34.8 km/h excluding idle)
- Maximum speed: 81.6 km/h

3.2 Data Processing

3.2.1 Pre-Processing Phase

The pre-processing phase consists in the following steps:

1. Input variables acquisition: Vehicle architecture
2. Battery sizing
3. Engine sizing
4. Components maps generation
5. Configuration space definition
6. Components requirements
7. Feasibility check on speed, power, battery and components requirements

The problem has been study both in space and in time domain. The space domain has been discretized according to the *Configuration Matrix Approach*, while the time domain according to the *Interval-Grid Approach*.

Configuration space

A configuration is defined as the combination of:

- *a gear number (GN)*: Number of gear ratios of the transmission - 6
- *a powerflow (PF)*: user-defined according to Table 3.1 - 8
- *an engine state (ES)*: Engine ON/OFF - 2

PF and GN are defined as *control variables*, while the ES and the SOC represent the *state variables*. The configuration space is simply defined as:

$$S_{conf} = S_{GN} \cdot S_{PF} \cdot S_{ES} \quad (3.4)$$

while the whole number of possible configuration is:

$$N_{conf} = N_{GN} \cdot N_{PF} \cdot N_{ES} = 96 \quad (3.5)$$

Such set of configurations is analysed by the optimization tool at each time step in order to set the optimal configuration that minimize the objective function.

Time Grid

The *Interval-Grid Approach* assumes the control variables to be constant over the entire interval, while the state variables are evaluated at the extremes of each interval by means of zero-dimensional kinematic equations. The intermediate variables are computed thanks to linear interpolation. The velocity time history of the dynamic model and the road slope are the input variable in the kinematic model. This procedure guarantees the vehicle ability to satisfy the required power demand.

The computational grid is subdivided in N_{int} intervals whose length is determined in order to reduce the size of the problem, i.e. the number of time steps. Each time interval has finite length of 1 second. The configuration matrix associated to a specific variable is $N_{int} \cdot N_{conf}$ matrix, which contains the values of the inherent variable at each instant for each possible configuration. Hence, it is possible to consider the physical discontinuity that could occur at each node, reducing the simulation time and the memory requirements.

Components generation and sizing

Following the input definition, the engine and the electric machine map are generated considering the reference map provided in the tool [25] by its respective manufacturers, by means of a scaling factor (SF):

$$\begin{cases} SF_{EM} = \frac{P_{peak,EM}}{P_{peak,ref,EM}} \\ SF_{ICE} = \frac{V_{ICE}}{V_{ICE,ref}} \end{cases} \quad (3.6)$$

Lithium-ion battery pack [25] is sized according to the maximum power of all the electric machine and the PE ratio defined by the user in the Architecture definition, i.e. the model input. Generally speaking, battery pack can be sized with two main approaches:

- *Kinematic approach*: Battery pack is sized in order to withstand with the power required from motion, given the vehicle speed
- *Tolerance approach*: in which the battery pack is sized according to a tolerance operating range based on the type of mission to be performed

Then, is well-known from course in electronics, that a battery pack is made up by a set of reference *cells* in series, characterized by constant nominal voltage and whose specifications are an input to the tool, which form the reference *unit*. A set of units in parallel, holding the same electrical capacity, define a *battery module*. A set of battery module in series define the required *battery pack*. The whole assembly has been depicted in Figure 3.10.

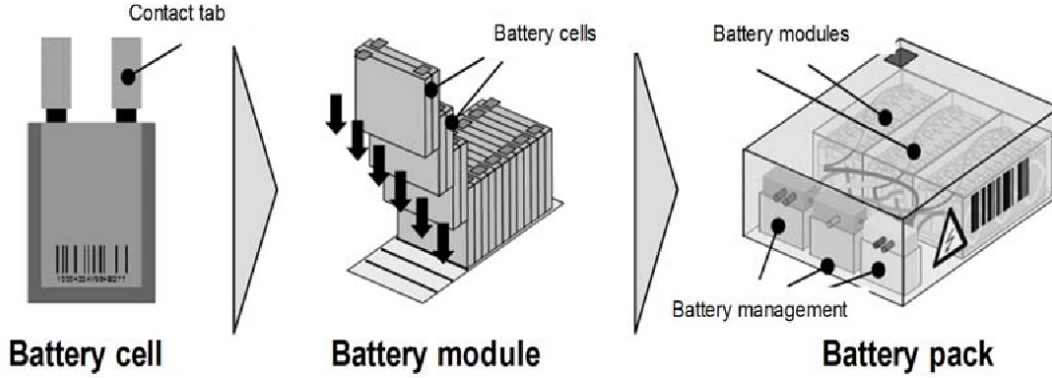


Figure 3.10: Battery pack

The input parameters provided by the optimization tool have been listed in Table 3.2:

Cell nominal voltage [V]	3.6
Number of cells in a unit	6
Cell capacity [Ah]	2.9
Battery nominal voltage [V]	300
Battery mass [kg]	170
Overall number of cells	1680
Coulomb efficiency [%]	100

Table 3.2: Battery input from optimization tool

The nominal energy of the battery is determined from the architecture parameters as the ratio between the electric machine peak power and the nominal PE ratio:

$$E_{batt} = \frac{EM_{power,tot}}{PE_{ratio_{nom}}} \quad [Wh] \quad (3.7)$$

Then the number of parallel units in each module, which hold the same capacity:

$$C_{batt} = E_{batt}/V_{batt,nom} \quad [Ah] \quad (3.8)$$

$$N_{pu} = C_{batt}/\text{Cell Capacity} \quad [-] \quad (3.9)$$

where C_{batt} is the battery capacity while N_{pu} is the number of parallel units. Then the number of modules in series, with constant voltage, follows:

$$V_{unit} = V_{module} = V_{cell} \cdot N_{cell} \quad [V] \quad (3.10)$$

$$N_{sm} = V_{batt,nom}/V_{module} \quad [-] \quad (3.11)$$

$$V_{batt} = V_{module} \cdot N_{sm} \quad [V] \quad (3.12)$$

$$N_{tot} = N_{sm} \cdot N_{cell} \cdot N_{pu} \quad [-] \quad (3.13)$$

$$R_{batt} = R_{module} \cdot N_{sm} \quad [\Omega] \quad (3.14)$$

which are the voltage per unit, the number of modules in series, the overall voltage of the battery, the overall number of cells in the battery and the battery electrical resistance, respectively.

Finally, the tool accounts for Li-on battery fading and compute the total battery mass considering an additional weight given by the Battery Management System (BMS) - which provides the battery cooling - as:

$$m_{batt} = 1,7 \cdot m_{batt,ref} \cdot \frac{N_{tot}}{N_{tot,ref}} \quad [kg] \quad (3.15)$$

The battery is modelled as an equivalent resistance circuit at constant temperature, with the inherent open-circuit voltage and resistance computed by interpolating a 1D map generated on the basis of the previous quantities and the input parameters, and based on battery SOC functions as follows:

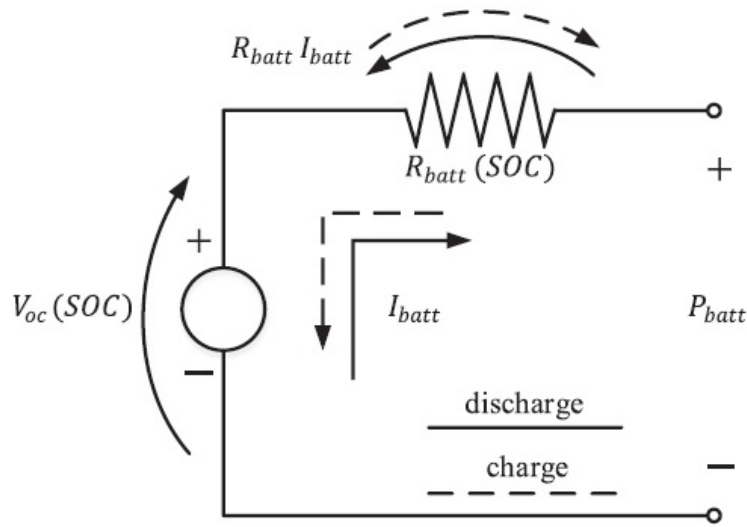


Figure 3.11: Battery equivalent model

$$V_{oc}(SOC) = V_{oc,base}(SOC) \cdot N_{sm} \cdot N_{cell} \quad [V] \quad (3.16)$$

$$R_{eq}(SOC) = R_{eq,ref}(SOC) \cdot \frac{N_{sm} \cdot N_{cell}}{N_{pu}} \quad [\Omega] \quad (3.17)$$

The maximum battery power is bounded by the *maximum power transfer theorem* and considering electro-chemical phenomena, hence:

$$P_{max,el}(SOC) = \frac{V_{oc}(SOC)^2}{4 \cdot R_{eq}(SOC)} \quad [W] \quad (3.18)$$

$$P_{chem}(SOC) = V_{oc}(SOC) \cdot \frac{C_{batt,dis}}{1h} \cdot C_{rate_{dis,max}} - R_{eq}(SOC) \cdot \left(\frac{C_{batt,dis}}{1h} \cdot C_{rate_{dis,max}} \right)^2 \quad (3.19)$$

During the optimization, the power limit curves together with $V_{oc}(SOC)$ and $R_{eq}(SOC)$ are used to determine the SOC variation and feasibility due to a given battery power demand.

$$I_{batt} = \frac{V_{batt} - \sqrt{V_{batt}^2 - 4 \cdot R_{batt} \cdot P_{batt}}}{2 \cdot R_{batt}} \quad (3.20)$$

$$SOC_t = SOC_{t-1} - \int \frac{I_{batt}}{C_{batt}} dt \quad (3.21)$$

Kinematic driveline and power unit mapping, instead, are computed according to vehicle dynamics equations. The total power demand required for motion Pr is derived from its multiple contribution - road grade resistance, driveline inertia, aerodynamic drag and rolling resistance - and its sign defines the traction-braking working asset of the vehicle [20]:

$$\begin{cases} Pr_{grade} = m_{veh} \cdot g \cdot \sin \alpha_r \cdot v_{veh} \\ Pr_{inertia} = \left(m_{veh} + \frac{I_{wh}}{R_{wh}} \right) \cdot v_{veh} \cot \dot{v}_{veh} \\ Pr_{aero} = \left(1/2 \cdot \rho_{air} \cdot c_x \cdot A_{veh} \cdot v_{veh}^2 \right) \cdot v_{veh} \\ Pr_{roll} = m_{veh} \cdot g \cdot \cos \alpha_r \cdot v_{veh} \quad \text{yields} \end{cases} \quad (3.22)$$

$$Pr = Pr_{grade} + Pr_{inertia} + Pr_{aero} + Pr_{roll} \quad (3.23)$$

where

- m_{veh} is the vehicle mass
- α_r is the road inclination
- v_{veh} is the vehicle speed
- I_{wh} is the wheel inertia
- R_{wh} is the dynamic wheel radius
- ρ_{air} is the air density
- c_x is the aerodynamic drag coefficient in the direction of motion
- A_{veh} is the vehicle frontal area

3.3 Post Processing

Multiple scripts are available in [25] for the post-processing task. The main issue regarding HEVs control strategies is to correctly compare the simulations outcome about the same reference in terms of fuel economy and CO_2 emissions. To do so, the following section will deal with the implementation of this correction task derived from international standard.

Equivalent CO_2 Emission and Equivalent Fuel Consumption Tank-to-Wheel

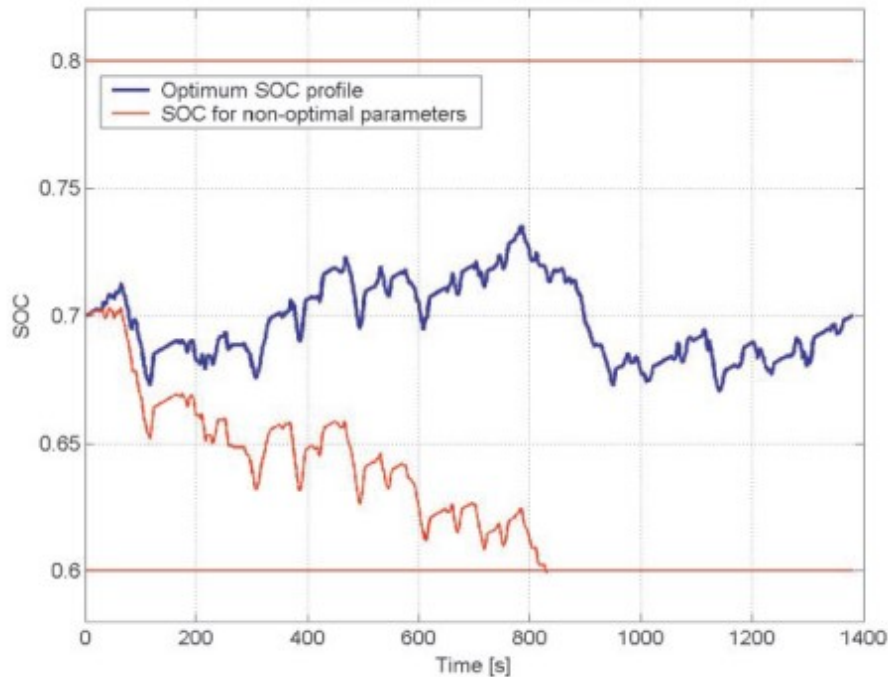


Figure 3.12: SOC at the end of the mission

Figure 3.12 highlights a key-point of the post-processing phase. It is clear that one of the main tasks of HEVs control strategies is to guarantee that at the end of the mission the battery state of charge SOC_f should be equal - or closer, at least - to the initial state of reference SOC_0 . This cannot always be ensured since the vehicle behaviour is influenced either by internal and environmental aspects that cannot always be predicted. In order to correctly compare architectures and configurations that guarantee at the same time, over the whole set of layouts tested:

- The minimum fuel consumption and CO_2 emission
- A final SOC level equal or closer to the reference
- A SOC window closer to the reference SOC value
- A charge-sustainability SOC trend over the entire mission

the ECE/trans/180/Add.15 regulation standard [28] has been implemented in the post-processing section of the algorithm. It prescribes the computation of the *equivalent CO_2 emission* and the *equivalent fuel consumption* to take into account the fuel that

would have been consumed to take the battery SOC at the initial value when the final SOC level at the end of the cycle is lower than the reference one. The regulation has been prescribed for WLTP procedure but the core has been extended to the other driving cycles adopted in this work. Then a correction factor has been evaluated for each single layout (defined by the Architecture Parameters) and obtained by varying only the EFs for a fixed driving cycle (WHVC, FTP 72, JC08 in the present work), using as design parameters n-pairs of EFs corresponding to n-configurations. An example is reported in Figure 3.13 and Table 3.3.

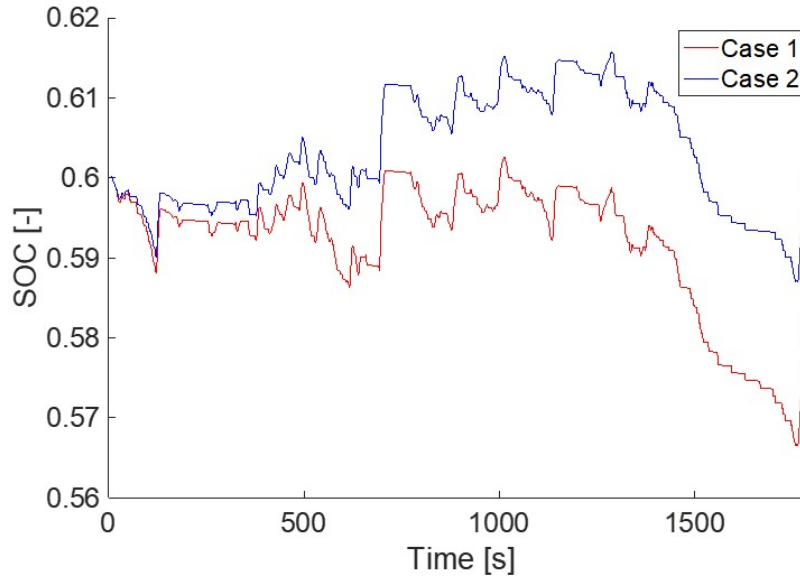


Figure 3.13: Example for $CO_{2,ttw}$ evaluation

Case 1	SOC _{final} [-]	$CO_{2,ttw}$ [g/km]	$CO_{2,ttw,eq}$ [g/km]
1	0.5812	329.9	341.4
2	0.6017	339.4	339.4

Table 3.3: Example for $CO_{2,ttw}$ correction and evaluation

Looking at Case 1, the final $CO_{2,ttw}$ value, i.e. the gross one, would set a condition to consider it as the optimal condition for the controller in terms of emissions, even if the final SOC value is lower than the reference. The Case 2, as well, would define a-priori an higher gross emission with respect to Case 1 but, at the end of the mission, the SOC is higher than the reference, which means that the A-ECMS controller conditions of charge-sustaining and SOC closer to the reference have been satisfied. By considering the equivalent CO_2 emission, the evaluation of the optimality is even more clear. The correction is applied only when the final SOC value is lower than the reference so that, at the end of the day, the net emission is higher for Case 1 with respect to Case 2, implying the optimality for the latter.

The corrected values of $CO_{2,ttw,eq}$ and $FC_{ttw,eq}$ must be calculated at the end of each phase of the test driving cycle starting from the following regression coefficient:

$$k_{CO_2} = \frac{n \cdot \sum (E_{REESS_i} \cdot CO_{2,ttw,i}) - \sum E_{REESS_i} \cdot \sum CO_{2,ttw,i}}{n \cdot \sum E_{REESS_i}^2 - (\sum E_{REESS_i})^2} \quad (3.24)$$

$$k_{fuel} = \frac{n \cdot \sum (E_{REESS_i} \cdot FC_{ttw,i}) - \sum E_{REESS_i} \cdot \sum FC_{ttw,i}}{n \cdot \sum E_{REESS_i}^2 - (\sum E_{REESS_i})^2} \quad (3.25)$$

where

- E_{REESS_i} is the electricity balance measured for the i-th Rechargeable Electric Energy Storage System [Wh/km]
- $CO_{2,ttw,i}$ is the tank-to-wheel emission measured for the n-th configuration [g/km]
- k_{CO_2} is the CO_2 emission correction coefficient [g/km/Wh/km]
- $FC_{ttw,i}$ is the fuel consumption measured for the n-th configuration [l/100km]
- k_{fuel} is the fuel consumption correction coefficient [l/100 km/Wh/km]

Then to account for the change in the energy content inherent to the on-board i-th Rechargeable Electric Energy Storage System, the regulation prescribes the following term:

$$\Delta E_{REESS_i} = 100 \cdot \frac{0.0036 \cdot RCB \cdot U_{REESS}}{E_{fuel}} \quad [-] \quad (3.26)$$

where

- RCB is the REESS charging balance over the phase [Ah] given by the battery capacity C_{tot} times the SOC variation within the considered phase
- U_{REESS} is the nominal REESS voltage [V]
- E_{fuel} is the energy content of the consumed fuel [MJ]

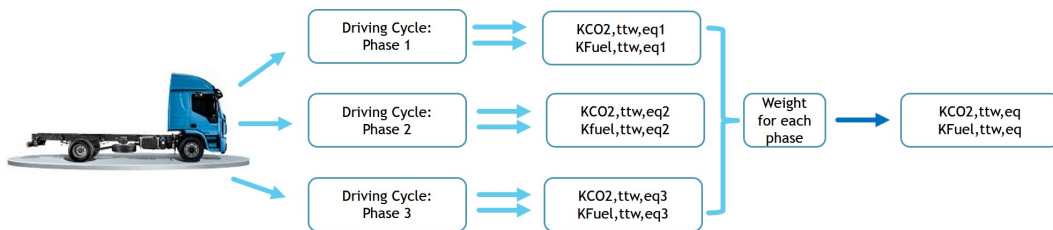


Figure 3.14: Correction coefficient evaluation procedure

Figure 3.14 highlights the procedure to retrieve the correction coefficients. These are determined for each phase of the driving cycle, e.g. urban, rural and motorway considering WHVC. Then a unique value for the whole driving cycle is stated by a weighted average based on the temporal duration of each phase.

Finally $CO_{2,ttw,eq}$ and $FC_{ttw,eq}$ are computed as:

$$CO_{2,ttw,eq} = CO_{2,ttw} - k_{CO_2} \cdot \Delta E_{REESS_i} \quad (3.27)$$

$$FC_{ttw,eq} = FC_{ttw} - k_{fuel} \cdot \Delta E_{REESS_i} \quad (3.28)$$

With reference to section 3.1.7 the following correction coefficients have been obtained for the driving cycles used for the testing campaign:

Driving Cycle	k_{CO_2} [g/km/Wh/km]	k_{fuel} [l/100 km/Wh/km]
WHVC	0.59660	0.02357
FTP-72	0.58947	0.02329
JC08	0.56726	0.02241

Table 3.4: Driving Cycle correction coefficients

Chapter 4

Control Strategy

The goal of the Adaptive formulation is to overcome the constraints given by the basic ECMS algorithm, in order to make the design parameters i.e., the Equivalence Factor (EFs), and the solution of its objective function cycle-independent ¹.

The problem of designing a real-time on-board implementable energy management strategy for hybrid electric vehicles and get, at the same time, a close-to-optimal solution has been the goal of extensive research over the last decade, as seen at the end of the previous chapter. In the following sections will focus the attention on the implementation of the Adaptive - ECMS with the aim of deriving the most suitable formulation for the case study under investigations. Multiple formulations are hereby proposed, either extracted from the literature or proposed in innovative solutions.

¹Recall: To guarantee the optimality and the charge-sustainability for any driving conditions, ECMS should know the cycle a-priori

4.1 Instantaneous A-ECMS formulation

The Instantaneous A-ECMS formulation is based on State of Charge (SOC) feedback from on-board batteries and has been derived from [6] and modified to be run on the optimization tool. The key-point of this strategy, highlighted in Equation 4.1, is to instantaneously change the value of the EFs in order to avoid the SOC deviation from the initial state, make it bounded about this value through a numerical formulation. The EFs correlation at the battery terminals then, makes the design parameters continuously dependent from each other, reducing the calibration complexity.

$$\begin{cases} s_{chg}(t) = s_{chg}(0) + \frac{s_{chg}(0) - s_{dis}(0)}{s_{chg}(0)} \cdot \frac{SOC_{high} - SOC(t)}{SOC_{high} - SOC_{low}}; & s_{dis}(t) = \frac{s_{chg}(t)}{\eta^2} \quad \text{if } SOC(t) < SOC_0; \\ s_{dis}(t) = s_{dis}(0) + \frac{s_{chg}(0) - s_{dis}(0)}{s_{dis}(0)} \cdot \frac{SOC_{high} - SOC(t)}{SOC_{high} - SOC_{low}}; & s_{chg}(t) = s_{dis}(t)\eta^2 \quad \text{if } SOC(t) > SOC_0; \end{cases} \quad (4.1)$$

This formulation has been demonstrated to be, either in literature and in results obtained:

- *Robust and reliable* as rely on SOC feedback and EFs obtained from the DoE
- *Easy to implement* as defined by known variables
- *Computationally cheap and stable*

4.2 Periodic A-ECMS formulation

The Periodic A-ECMS takes its origin from the work *Online energy management for hybrid electric vehicles (2008)* [23] by Kessels, Koot et al. and following revision in the paper *Adaptive equivalent consumption minimization strategy for hybrid electric vehicles (2010)* [24] by Onori S., Serrao L. and Rizzoni G.. In [23] an adaptation law based on a proportional-integral (PI) controller of the type shown in Equation 4.2 was proposed:

$$s(t) = s_0 + k_p \cdot (SOC_0 - SOC(t)) + k_i \int_0^t (SOC_0 - SOC(\tau)) d\tau \quad (4.2)$$

where s_0 , k_p and k_i are the generic EF of initialization, the proportional and the integral gains of the control law, respectively. The drawback of this formulation was evidenced in the lack of ability of the battery to fully exploit its entire operating range [23], driven by the attitude of the controller to instantaneously correct any small SOC deviation from the target one. To allow the battery to span over a wider range of SOC, in [24] and [19] a discrete formulation have been introduced as follows in Equation 4.3:

$$\begin{cases} s_{dis}(t) = \frac{s_{dis}(t-T) + s_{dis}(t-2T+1)}{2} + k_p \cdot (SOC_0 - SOC(t)) + k_i \int_0^t (SOC_0 - SOC(\tau)) d\tau \\ s_{chg}(t) = \eta^2 \cdot s_{dis}(t) & \text{if } t=p \cdot T, \text{ with } p \in \mathbb{N} \\ s_{dis}(t) = s_{dis}(t-1); \quad s_{chg} = s_{chg}(t-1) & \text{otherwise} \end{cases} \quad (4.3)$$

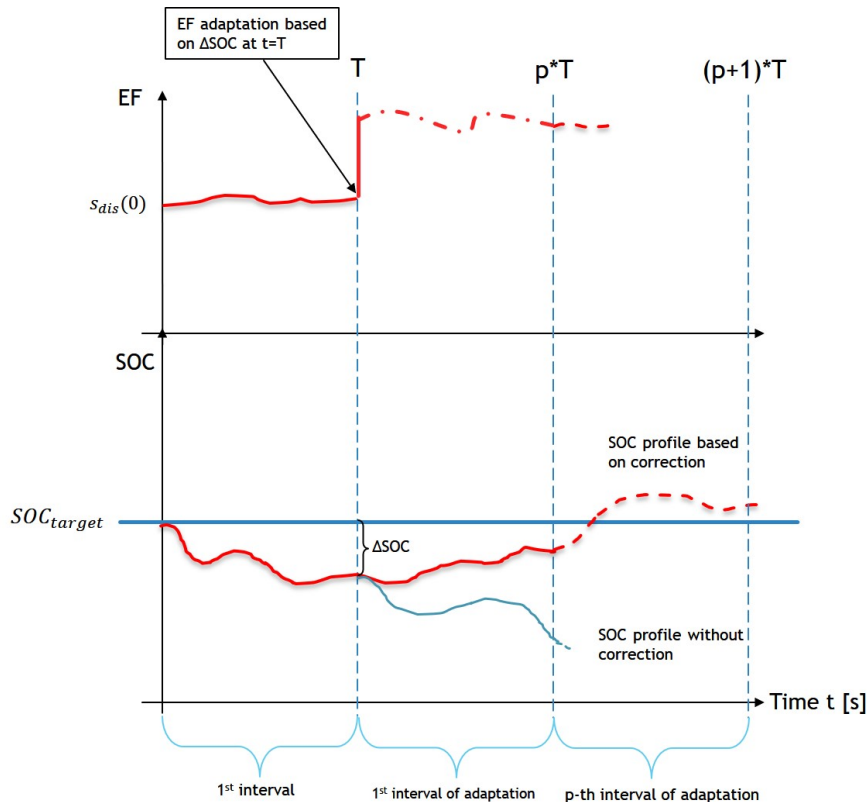


Figure 4.1: Periodic Adaptation Law

The algorithm proposed in the set of Equations 4.3 and represented in Figure 4.1 should be interpreted in this way: once the algorithm has been initialized by the EFs derived from DoE, the adaptation law update the EFs at regular time intervals, periodically tuning their value. The correction is driven by both a proportional and integral controller, which tune the discharge coefficient.

The former implies a correction proportional to the error i.e., the SOC difference from the target value at the periodic instant T , and provides a large corrective action correction when the instantaneous errors are large. Its main drawback is that it might introduces a lack of precision when the phenomenon under control holds high variation frequencies, implying the so-called *overshoot* - the system is too stiff and provides a correction which is larger than needed.

The latter accounts for the SOC temporal evolution by means of an integral gain. It reacts to the accumulation of errors and causes a slow-reacting control action. Its disadvantages are mainly that it is insensitive to high frequencies and prone to cause instability [22].

This solution is computationally cheaper with respect to the instantaneous formulation, while the main handicap is given by a higher amount of calibration parameters i.e., $(s(t), T, k_p, k_i)$. The control input so defined can be written as:

$$u_c = k_p \cdot \left((SOC_0 - SOC(t)) + \frac{1}{T} \int_0^t (SOC_0 - SOC(\tau)) d\tau \right) \quad (4.4)$$

where the term $T = \frac{k_p}{k_i}$ is defined as *reset time* and admits the correlation between the two gains, reducing the calibration complexity and setting a control time consistent with the gains adopted. The charge coefficient is then obtained by the correlation at battery terminals. Within the discretized time windows, the EFs are kept constant. Finally, to increase the robustness and the stability of the controller, EFs have been bounded between the interval $s_{chg,min} = 2$ and $s_{dis,max} = 3$, which have been demonstrated to be, either by literature and simulation performed, the more suitable to get a stable and optimal solution.

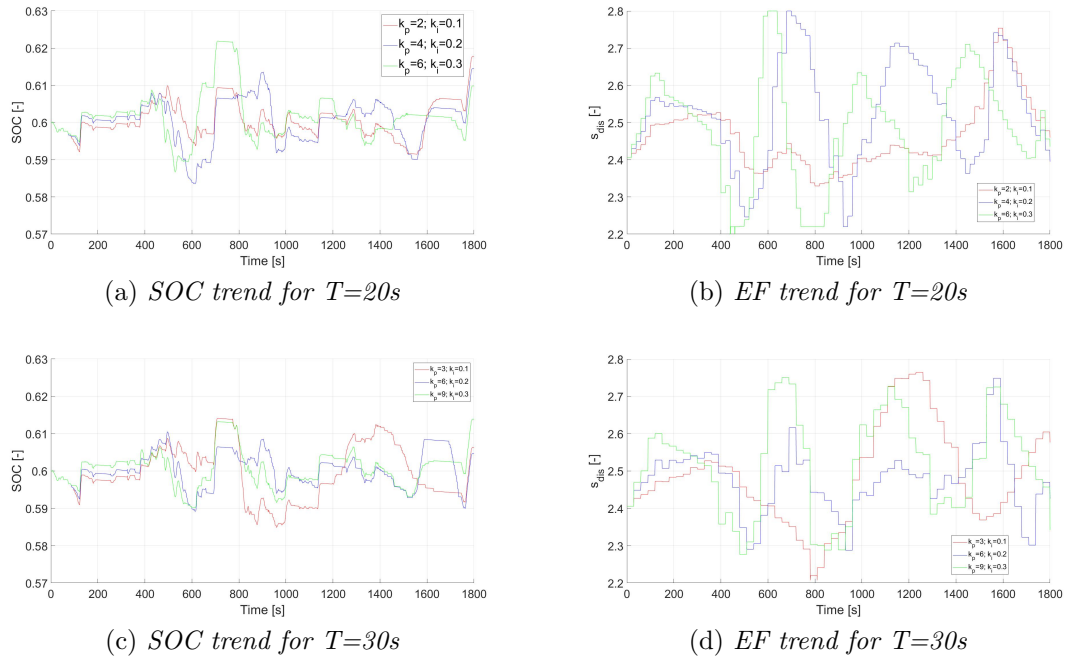


Figure 4.2: Sensitivity Analysis of the Periodic Controller Gains - $T=20s$ and $T=30s$

From Figures 4.2 (a) and (c), it is noticeable that by adopting reasonable values for the reset time a narrow SOC window could be obtained for time intervals between 20s and 30s. The latter case, in particular, shows a narrower SOC window and a charge-sustaining behaviour more evident with respect to the former. As stated in the previous paragraph, larger proportional gain must be tuned by larger integral gain, otherwise an intrinsic unstable behaviour might be introduced from the controller. This can be easily solved by the after-mentioned EFs saturation that it is clearly visible in Figures 4.3 (b) and (d) for the same time frames.

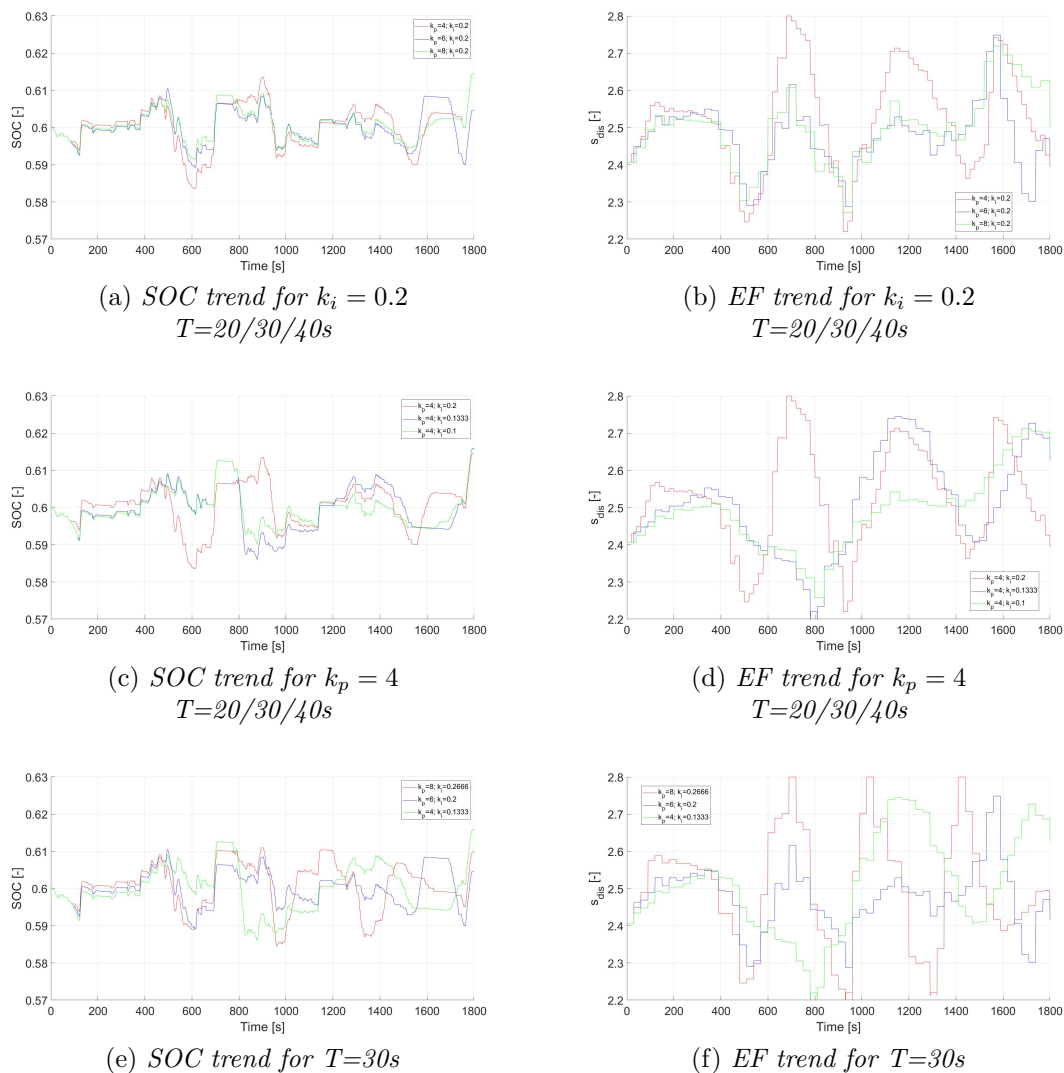


Figure 4.3: Sensitivity Analysis of the Periodic Controller Gains - WHVC

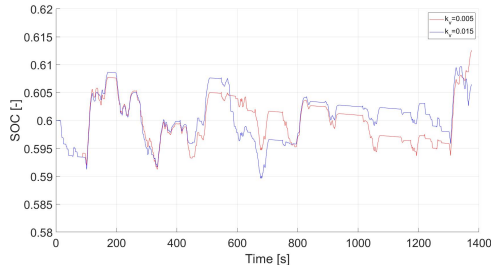
By making reference to WHVC Test Procedure, by increasing k_p for $k_i = const$, the time interval of adaptation increases according to the reset time definition. As detectable from Figure 4.3 (b) this leads to a lower oscillation of the discharge factor (hereby representative also for the charging factor, given the correlation at battery terminals), which means a stiffer controller with respect to SOC deviation from reference and less variation in battery management. Moreover, the higher k_p the better is the charge-sustaining attitude of the controller (Figure 4.3 (a)) On the other hand, increasing the time interval of adaptation means making the controller less responsive to sudden SOC and torque requests variations. Thus, a trade-off between controller stiffness and update must be checked. Then from Figures 4.3 (c) and (d), is noticeable that by lowering k_i for $k_p = const$, the time frame of adaptation is wider, as expected. By definition, k_i causes a slow-reacting control action and smaller value can stabilize the SOC window reducing the drifts from the reference, even if the EF does not assume cyclic values as happen for higher k_i , increasing its uncertainty in the long term. Finally, from Figures 4.3 (e) and (f) you can highlight that for $T=const$, according to the previous statements, the best choice of controller gains can be obtained by using trade-off values for k_p and k_i as 6 and 0.2, respectively, to ensure optimal trends either for SOC and EF.

4.3 Hybrid A-ECMS formulation

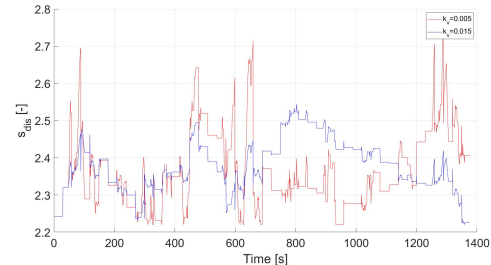
In the current section, a new adaptive formulation will be introduced. The idea behind is to combine the potentials of the periodic adaptivity proposed in [19], in which the computational time is lower than the instantaneous formulation and the adaptation law is driven by a controlled linear system, with a further correction which accounts for a sudden increase of torque requested by the driver or a strong deceleration, that can strongly affect the battery SOC - depleting it or increasing it, respectively. The latter implies a vehicle speed controller that instantaneously update the EFs based on the instantaneous speed difference as proposed in [18]. Summing up, the proposed strategy is reported in the Equation set 4.5:

$$\begin{cases} s_{dis}(t) = \frac{s_{dis}(t-T) + s_{dis}(t-2T+1)}{2} + k_p \cdot (SOC_0 - SOC(t)) + k_i \int_0^t (SOC_0 - SOC(\tau)) d\tau \\ s_{chg}(t) = \eta^2 \cdot s_{dis}(t) & \text{if } t=p \cdot T, \text{ with } p \in \mathbb{N} & \text{otherwise} \end{cases}$$

$$\begin{cases} s_{dis}(t) = s_{dis}(t-1); & \text{if } \Delta \bar{v} > 1 \text{ km/h}; k_v = 0 \\ s_{chg}(t) = s_{chg}(t-1) \\ s_{dis}(t) = s_{dis}(t-1) + k_v \cdot (v(t) - v(t-1)); & \text{if } \Delta \bar{v} < 1 \text{ km/h}; k_v = const \\ s_{chg}(t) = s_{chg}(t-1) + k_v \cdot (v(t) - v(t-1)) \end{cases} \quad (4.5)$$



(a) SOC trend



(b) EF trend

Figure 4.4: Speed proportional gain for $s_{dis,0} = const$

From Figure 4.4 can be extracted similar conclusions to those seen in the previous section, plus that lower k_v are required for urban-kind missions in order to guarantee the SOC stability over the reference and avoiding the controller overshoot.

Chapter 5

Results

The results of the implementation will be analysed according to the fitting with respect to the benchmark provided by the Dynamic Programming optimization algorithm. The equivalence factor reported will be the one used for the strategy initialization. The optimal strategy will be choice with reference to the $CO_{2,ttw,eq}$ *engine-out* emission seen in Section 3.3, the SOC at the end of the mission, the ΔSOC window and the powerflow strategy extracted by the controller. Moreover, a sensitivity analysis will be carried out on each driving cycle, comparing the best and the worst case scenario to assess the robustness of the controller. Finally, to state the improvement with respect to the conventional version of the powertrain, the equivalent CO_2 reduction and Fuel Economy have been reported, making reference to the results highlighted in Table 5.1:

Driving Cycle	$CO_{2,ttw,DP}$ [g/km]	$CO_{2,ttw,PT}$ [g/km]	$FuelEconomy_{DP}$ [l/100km]
WHVC	337.86	393.55	15.55
FTP-72	332.25	449.54	17.76
JC08	327.33	403.37	16.62

Table 5.1: $CO_{2,ttw}$ and Fuel economy reference values for each driving cycle

5.1 WHVC

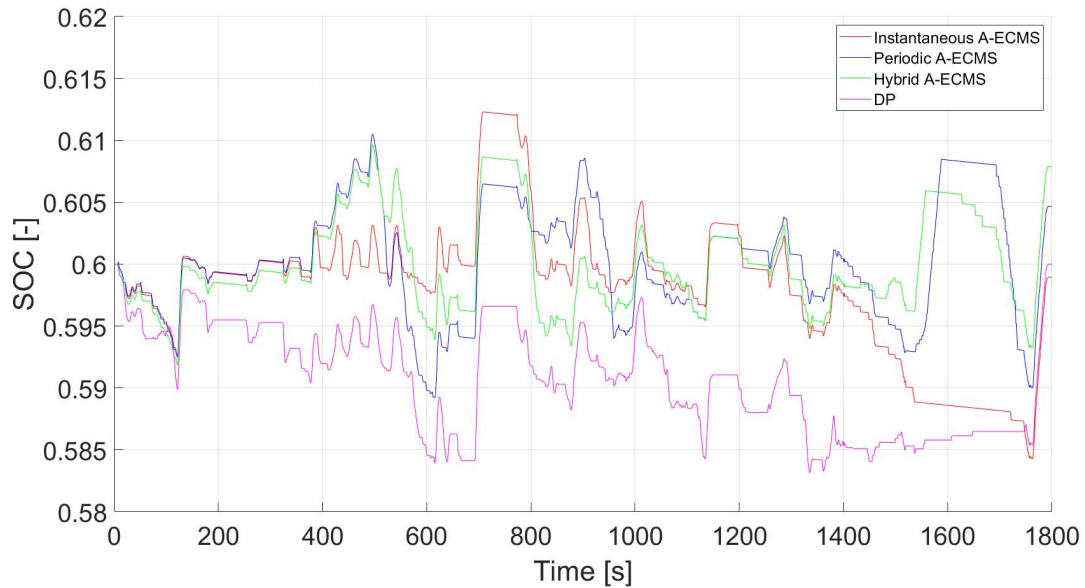


Figure 5.1: SOC profile on WHVC - Best case scenario

Quantity	Control Strategy			
	DP	Instantaneous	Periodic ($k_p=6, k_i=0.2$)	Hybrid ($k_p=6, k_i=0.2, k_v=0.015$)
$s_{chg}[-]$	-	2.2487	-	-
$s_{dis}[-]$	-	2.2341	2.4055	2.3132
$CO_{2,ttw}[g/km]$	337.86	338.33	342.60	343.31
$CO_{2,ttw,eq}[g/km]$	337.86	338.81	342.60	343.31
$FC_{ttw}[l/100km]$	13.35	13.37	13.54	13.56
$FC_{ttw,eq}[l/100km]$	13.35	13.39	13.54	13.56
$SOC_{final}[-]$	0.6000	0.5989	0.6047	0.6079
$SOC_{min}[-]$	0.5835	0.5843	0.5892	0.5918
$SOC_{max}[-]$	0.6000	0.6123	0.6105	0.6096
$\Delta CO_2\%DP$	0.0000	0.2811	1.394	1.613
$\Delta CO_2\%PT$	-14.15	-13.90	-12.95	-12.76
ΔSOC	0.000	-0.001	0.005	0.008
SOC Window	0.017	0.028	0.021	0.018

Table 5.2: Best case scenario on WHVC test cycle

With reference to Figure 5.1 and results reported in Table 5.2 for the best case scenario, the leading control strategy on WHVC has been performed by the instantaneous controller, even if the final SOC is under the reference. In this case the larger SOC window adopted, compared to other controllers, led to fully exploit the battery operating range for the majority of the driving cycle. The powerflow strategy, indeed, is similar to DP if we compare the SOC profiles depicted in Figures 5.4 (a) and (b), in which is also visible how the instantaneous controller is more prone to maintain a charge-sustaining behaviour until the start of the motorway phase - which is characterized by higher speeds, hence

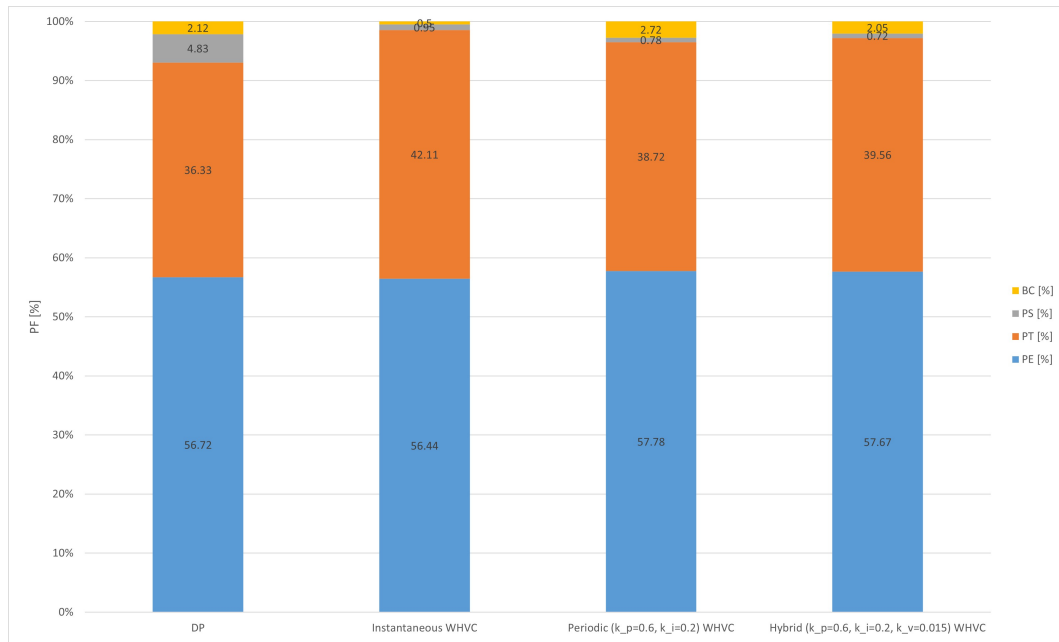


Figure 5.2: Powerflow strategies on WHVC for different controllers - Best case scenario

higher request of power - that made necessary to switch to the pure thermal mode, where the engine can be run at higher efficiencies, before ending up with a full battery charging. Higher emissions have been obtained both for the periodic and the hybrid controller, even if the fuel consumption and the CO_2 % difference with respect to the DP optimization is lower than 2%, given a higher amount of battery charging within the cycle. The best charge-sustaining behaviour over the whole cycle and the narrower SOC window, instead, has been performed by the hybrid controller.

Table 5.3 highlights the worst case scenario for the same controllers and test cycle, while Figure 5.3 shows a comparison in powerflow strategies for the best and worst case scenarios.

Quantity	Control Strategy			
	DP	Instantaneous	Periodic ($k_p=6, k_i=0.2$)	Hybrid ($k_p=6, k_i=0.2, k_v=0.015$)
$s_{chg}[-]$	-	2.4748	-	-
$s_{dis}[-]$	-	2.2248	2.6608	2.4343
$CO_{2,ttw}[g/km]$	337.86	358.86	350.05	349.91
$CO_{2,ttw,eq}[g/km]$	337.86	358.86	350.05	349.91
$FC_{ttw}[l/100km]$	13.35	14.18	13.83	13.83
$FC_{ttw,eq}[l/100km]$	13.35	14.18	13.83	13.83
$SOC_{final}[-]$	0.6000	0.6147	0.6159	0.6198
$SOC_{min}[-]$	0.5835	0.5986	0.5869	0.5875
$SOC_{max}[-]$	0.6000	0.6147	0.6159	0.6198
$\Delta CO_2\%DP$	0.0000	6.2155	3.6071	3.5670
$\Delta CO_2\%PT$	-14.15	-8.81	-11.05	-11.09
ΔSOC	0.000	0.0147	0.0159	0.0198
SOC Window	0.017	0.0161	0.0290	0.0323

Table 5.3: Worst case scenario on WHVC test cycle

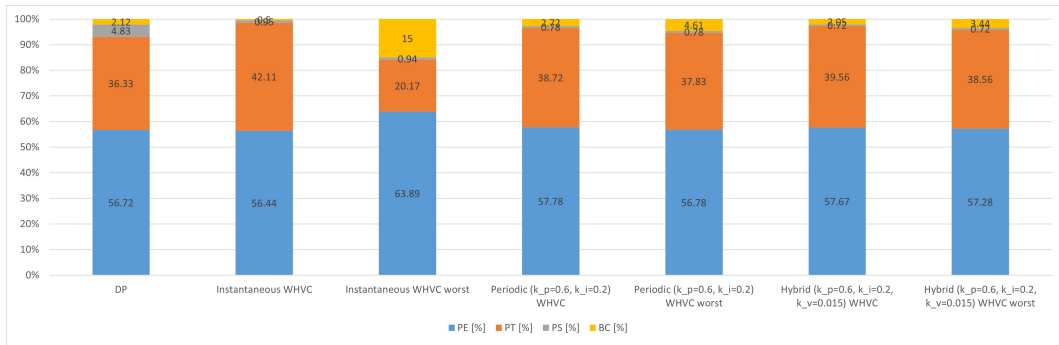


Figure 5.3: Powerflow strategies comparison on WHVC

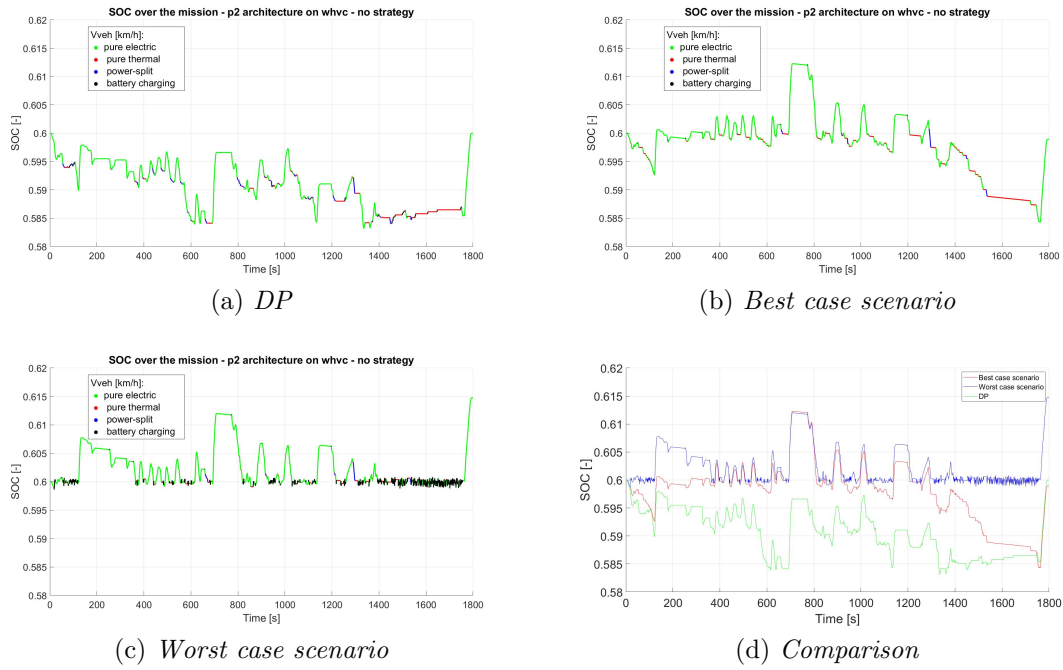


Figure 5.4: EMS comparison on WHVC - Instantaneous controller

Focusing on the instantaneous controller and by making reference to Figures 5.4 and 5.5, which show a comparison between the best and worst case scenario, the instantaneous controller in the latter made an intensive use (15 %) of the battery charging mode which led to an emission higher than 6% compared to DP and the former scenario. This can be driven by the higher weight chosen for the initialization charging factor, 2.4748 (worst) compared to 2.2487 (best), that is conditioned by a large oscillation over the mission while increasing the equivalent consumption given by the battery. This condition has been highlighted in Figure 5.5 (b), in which is also visible the unstable behaviour of the controller towards the end of the mission given the battery charging mode depicted in Figure 5.4 (c).

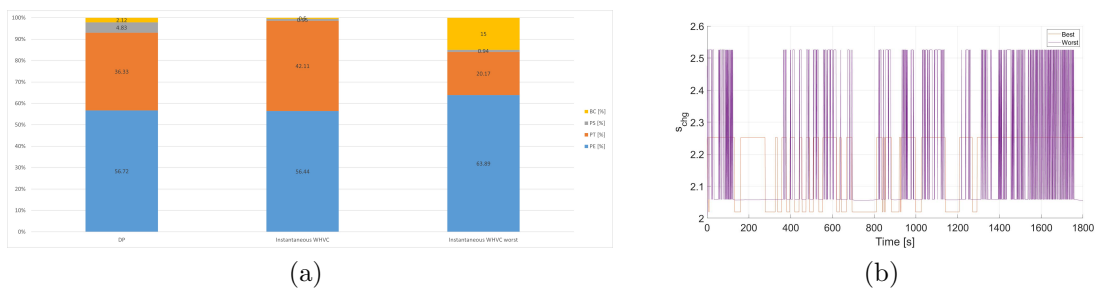


Figure 5.5: Powerflow strategies and charging factor comparison on WHVC - Instantaneous controller

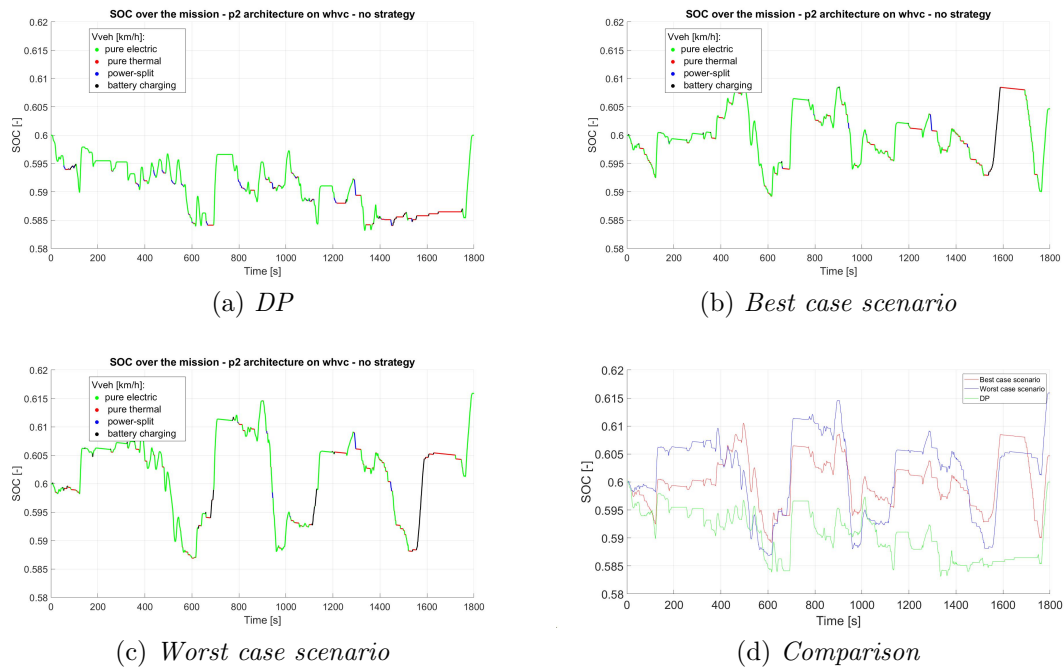


Figure 5.6: EMS comparison on WHVC - Periodic controller

In the following, similar comparison are reported either for the periodic and the hybrid controller, where the former performs a better strategy compared to the latter as stated before and on the basis of the results reported in Table 5.2.

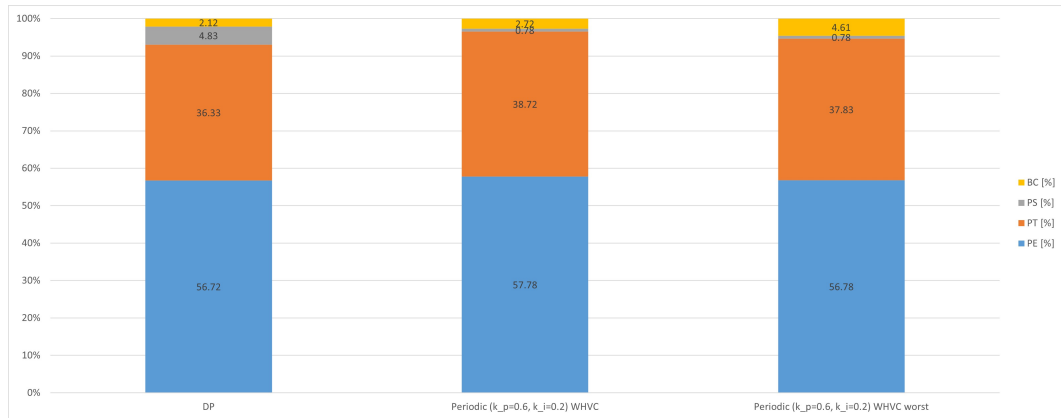


Figure 5.7: Powerflow strategies on WHVC - Periodic controller

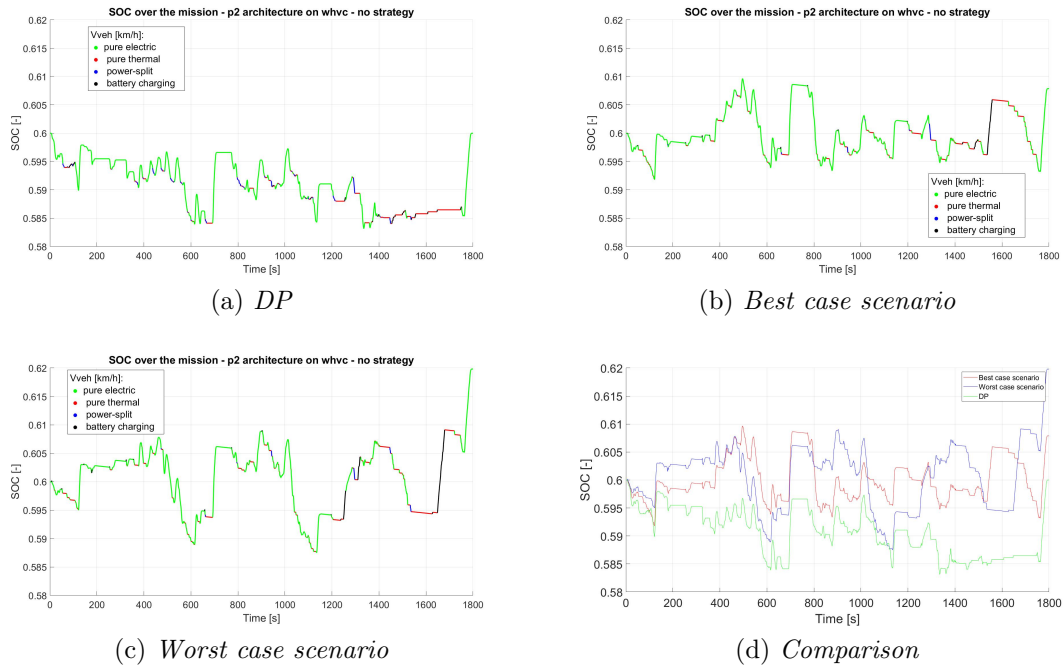


Figure 5.8: EMS comparison on WHVC - Hybrid controller

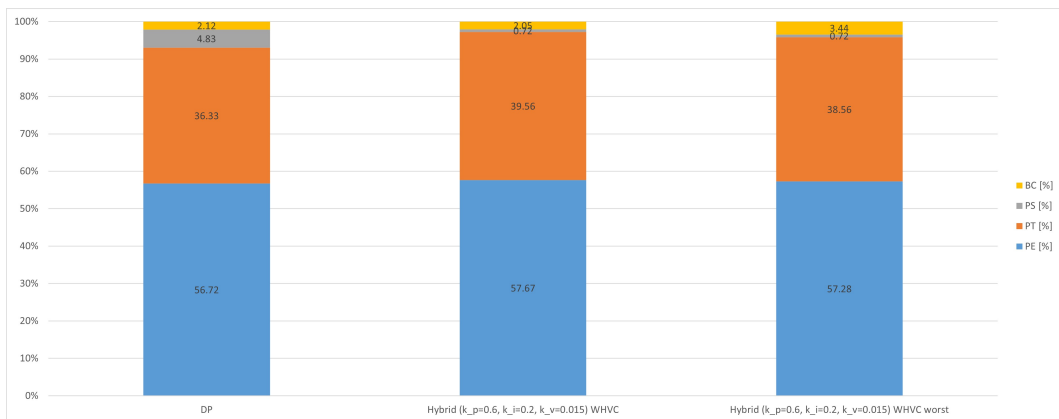


Figure 5.9: Powerflow strategies on WHVC - Hybrid controller

5.2 FTP-72

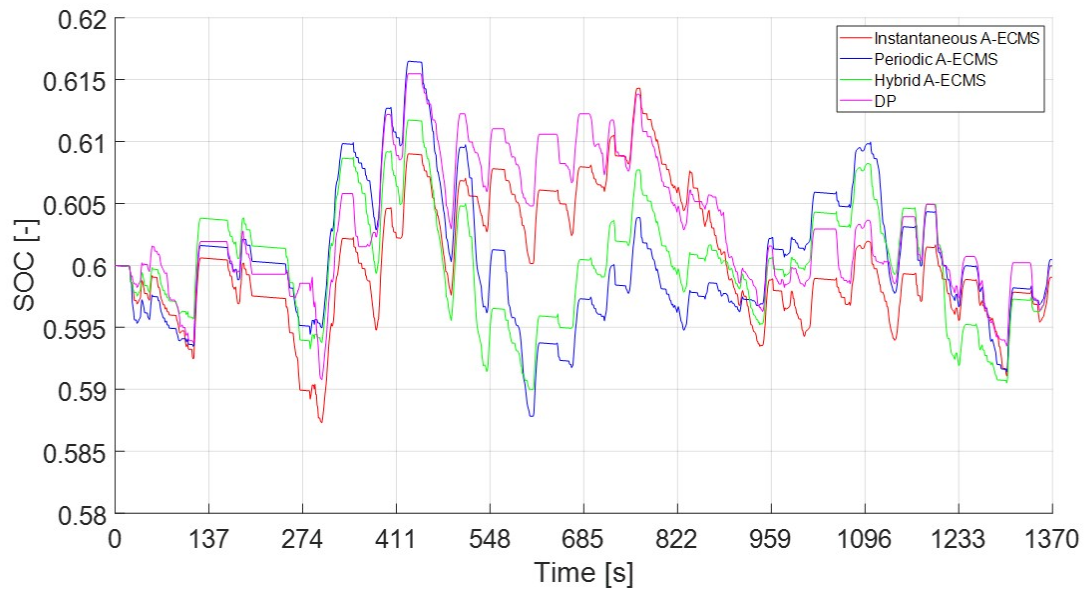


Figure 5.10: SOC profile on FTP72 - Best case scenario

Quantity	Control Strategy			
	DP	Instantaneous	Periodic ($k_p=6, k_i=0.2$)	Hybrid ($k_p=6, k_i=0.2, k_v=0.015$)
$s_{chg}[-]$	-	2.1617	-	-
$s_{dis}[-]$	-	2.3952	2.2842	2.3542
$CO_{2,ttw}[g/km]$	332.25	331.83	334.13	333.55
$CO_{2,ttw,eq}[g/km]$	332.25	332.56	334.13	333.62
$FC_{ttw}[l/100km]$	13.13	13.11	13.20	13.17
$FC_{ttw,eq}[l/100km]$	13.13	13.14	13.20	13.18
$SOC_{final}[-]$	0.6000	0.5990	0.6005	0.5999
$SOC_{min}[-]$	0.5908	0.5873	0.5878	0.5900
$SOC_{max}[-]$	0.6155	0.6143	0.6165	0.6117
$\Delta CO_2\%DP$	0.0000	0.0924	0.5650	0.4134
$\Delta CO_2\%PT$	-26.09	-26.02	-25.67	-25.79
ΔSOC	0.000	-0.0010	0.0005	-0.0001
SOC Window	0.025	0.027	0.029	0.022

Table 5.4: Best case scenario on FTP72 test cycle

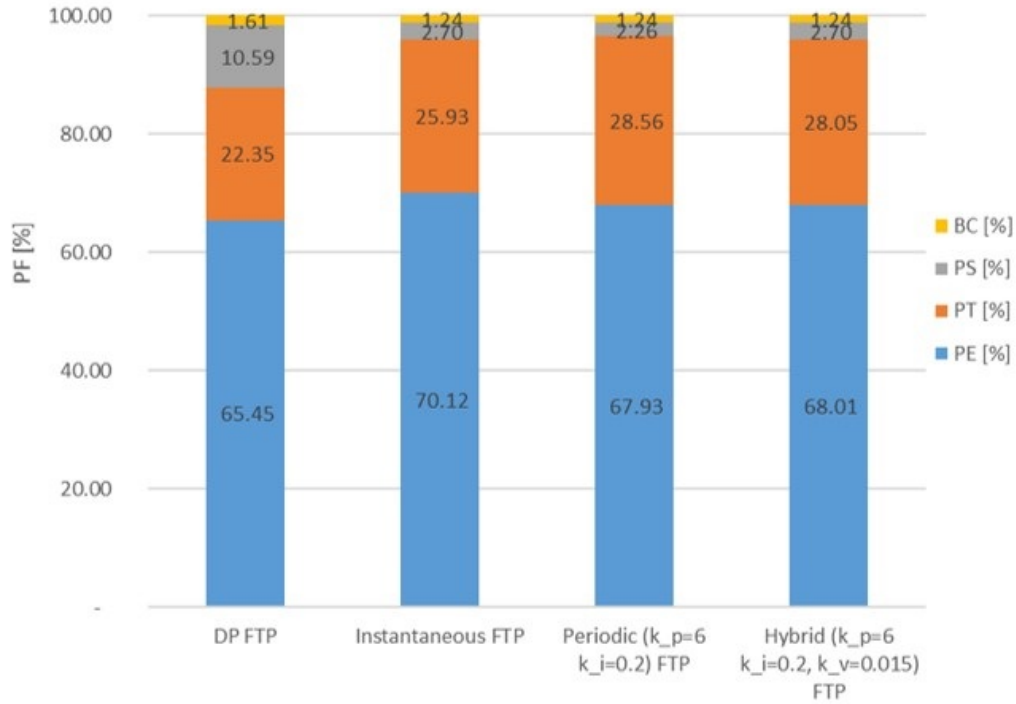


Figure 5.11: Powerflow strategies on FTP72 for different controllers - Best case scenario

Looking at Figure 5.10 and Table 5.4 can be deduced that the best case scenario for this driving cycle is obtained with the hybrid approach, which guarantee the best result in terms of charge-sustainability and final SOC, while a good compromise in terms of CO_2 emission is reached with a difference of less than 0.5% with respect to the dynamic programming. Moreover, it shows the narrower SOC window as seen for the WHVC case. The FTP-72 driving cycle is a reference cycle for the American market and is characterized by a urban phase and by a rural phase. This perhaps represents the type of route most frequently performed by the vehicle type under investigation, which is mainly adopted for massive transportation of building materials or wastes. Here the hybrid approach is more prone to adapt to the change of road type and mission, while the periodic strategy would deserve a lower update interval to keep the proper SOC window, hence increasing the computational effort. The instantaneous formulation follows a similar trend with respect to the dynamic programming but its EMS is more prone to use the battery in the urban phase (Figure 5.11), leading to a faster discharge in the short-track, with respect to the hybrid formulation that keeps its SOC about the reference. The whole set of controllers oscillate about the reference SOC value, exploiting a wide operating range of the battery.

As seen for WHCV, Table 5.5 highlights the worst case scenario for the same controllers on FTP-72, while Figure 5.12 shows a comparison in powerflow strategies for the best and worst case scenarios.

Compared to WHVC results, here the instantaneous formulation plays the worst strategy compared to the other controllers in the worst case scenario. Moreover, if compared with the hybrid strategy, the latter performs the best optimization either in the best and in the worst case scenario, stating its validity for the cycle under investigation.

Quantity	Control Strategy			
	DP	Instantaneous	Periodic ($k_p=6, k_i=0.2$)	Hybrid ($k_p=6, k_i=0.2, k_v=0.015$)
$s_{chg}[-]$	-	2.4997	-	-
$s_{dis}[-]$	-	2.2331	2.7604	2.7385
$CO_{2,ttw}[g/km]$	332.25	345.33	342.29	341.69
$CO_{2,ttw,eq}[g/km]$	332.25	345.33	342.29	341.69
$FC_{ttw}[l/100km]$	13.13	13.64	13.52	13.50
$FC_{ttw,eq}[l/100km]$	13.13	13.64	13.52	13.50
$SOC_{final}[-]$	0.6000	0.6072	0.6071	0.6068
$SOC_{min}[-]$	0.5908	0.5933	0.5867	0.5872
$SOC_{max}[-]$	0.6155	0.6186	0.6130	0.6130
$\Delta CO_2\%DP$	0.0000	3.94	3.02	2.84
$\Delta CO_2\%PT$	-26.09	-23.18	-23.86	-23.99
ΔSOC	0.000	0.0072	0.0071	0.0068
SOC Window	0.0247	0.0194	0.0263	0.0258

Table 5.5: Worst case scenario on FTP72 test cycle

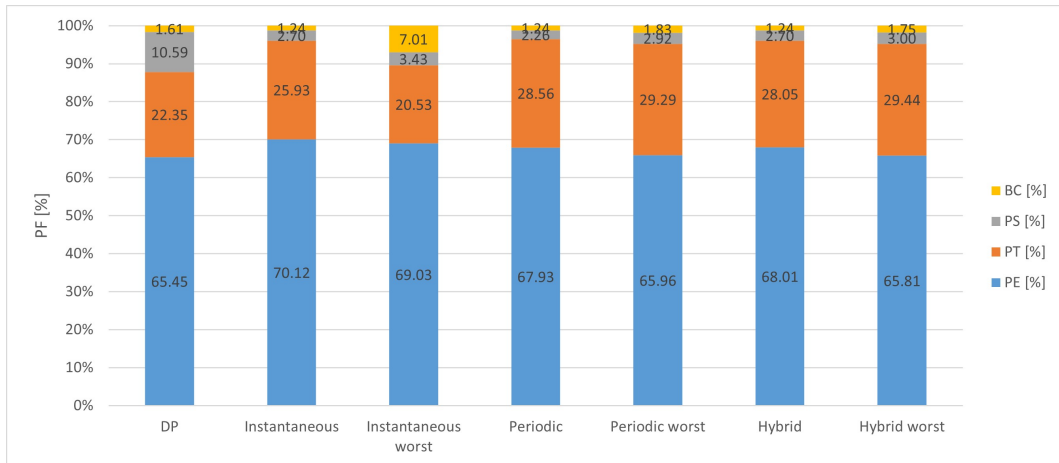


Figure 5.12: Powerflow strategies comparison on FTP72

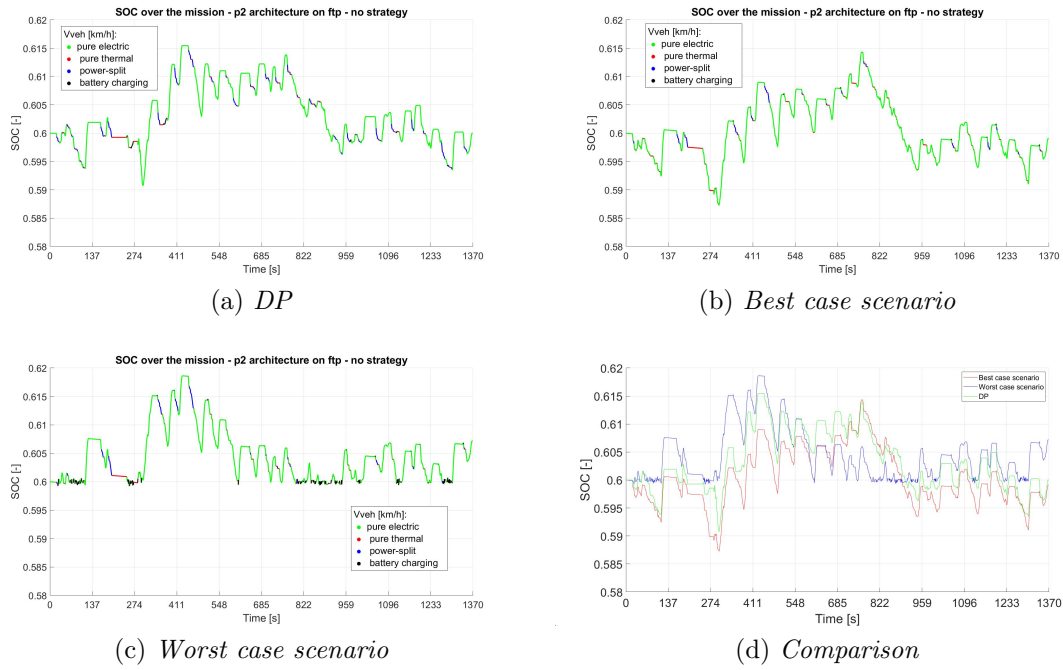


Figure 5.13: EMS comparison on FTP72 - Instantaneous controller

By looking at Figures 5.13 (c) and 5.14, a similar trend seen in the worst case scenario for the instantaneous controller on WHVC (Figure 5.4 (c)) is noticeable. This can be a proof of the cycle-independency of the controller and how the battery charging operating mode can be addressed as a fault of the controller strategy if frequently performed during the mission.

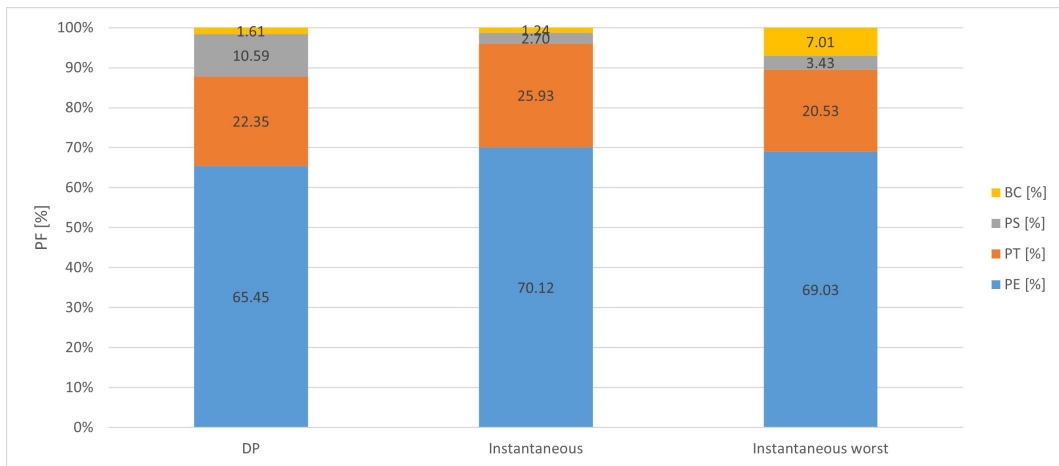


Figure 5.14: Powerflow strategies on FTP72 - Instantaneous controller

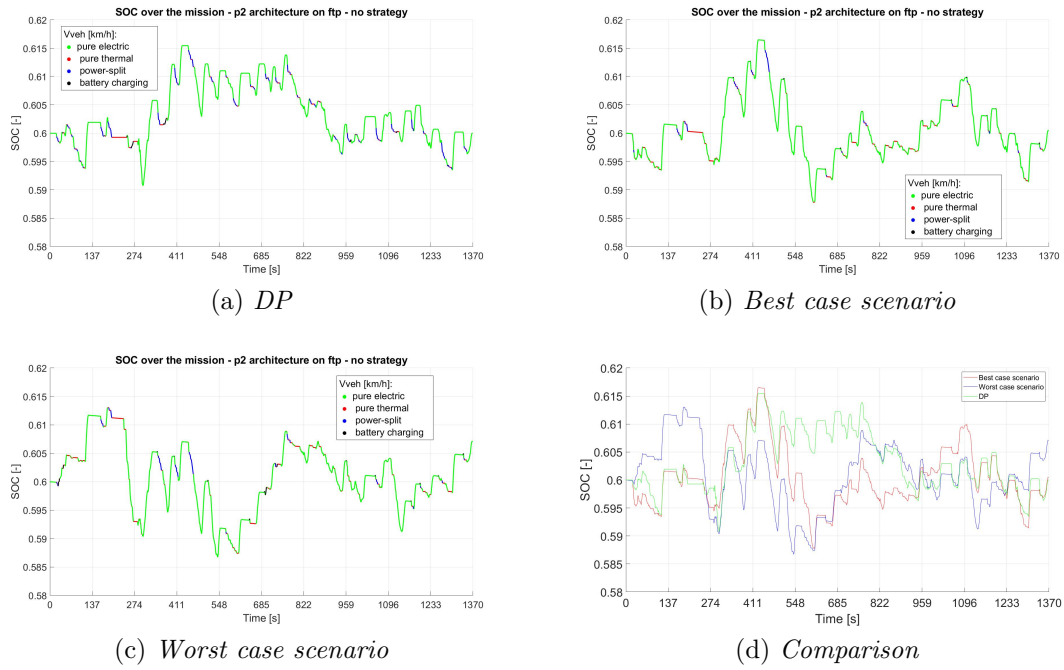


Figure 5.15: EMS comparison on FTP72 - Periodic controller

Generally speaking, the periodic controller shows the worst behaviour on FTP-72, if compared to other strategies.

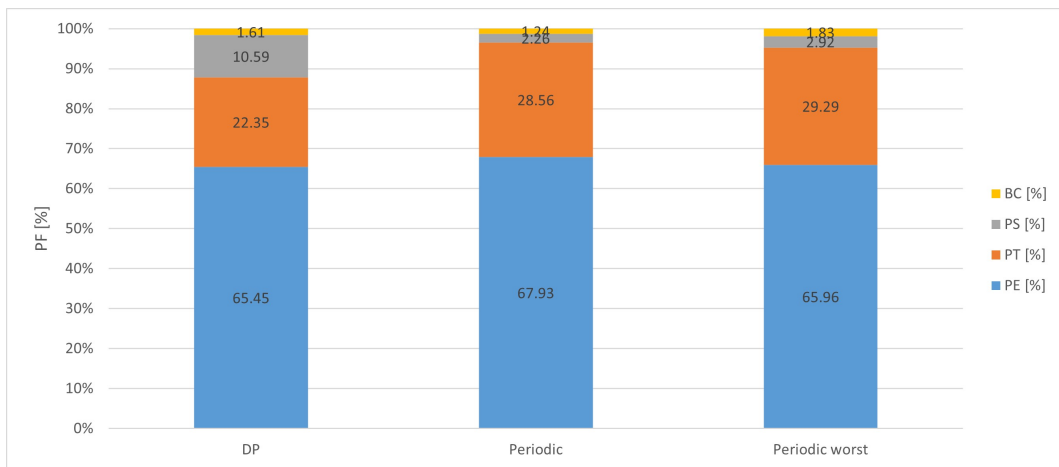


Figure 5.16: Powerflow strategies on FTP72 - Periodic controller

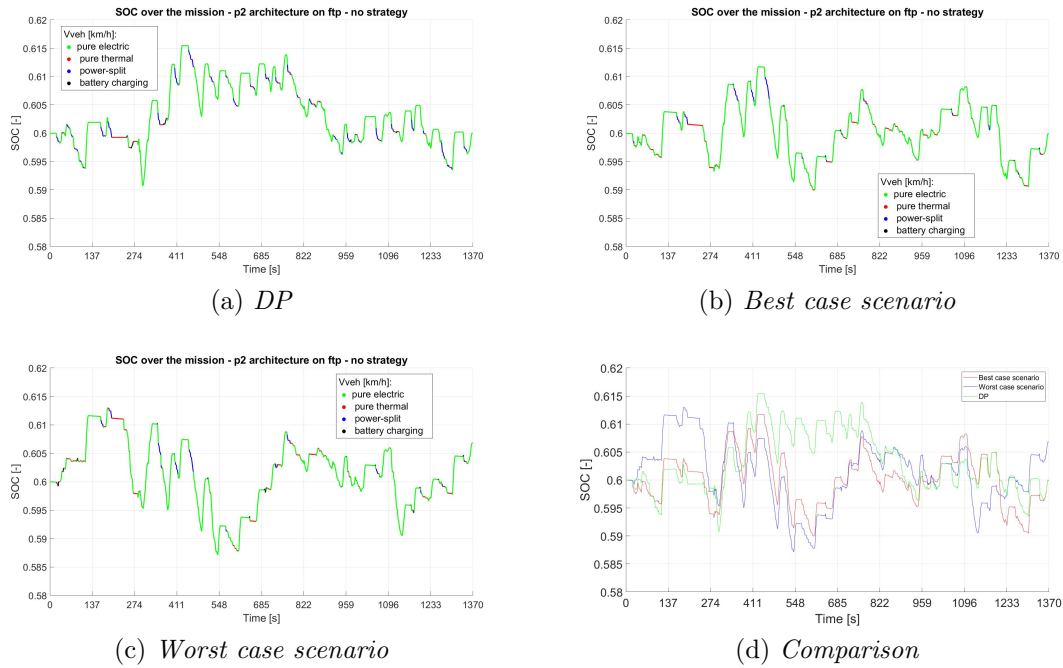


Figure 5.17: EMS comparison on FTP72 - Hybrid controller

Making reference to Figures 5.17 (a) and (b), we can see the wider SOC operating range performed by the hybrid strategy with respect to the Dynamic Programming optimizer, particularly in the middle of the driving mission in between the two phases of the cycle, where the EMS of the hybrid controller avoids to keep the battery away from the reference.

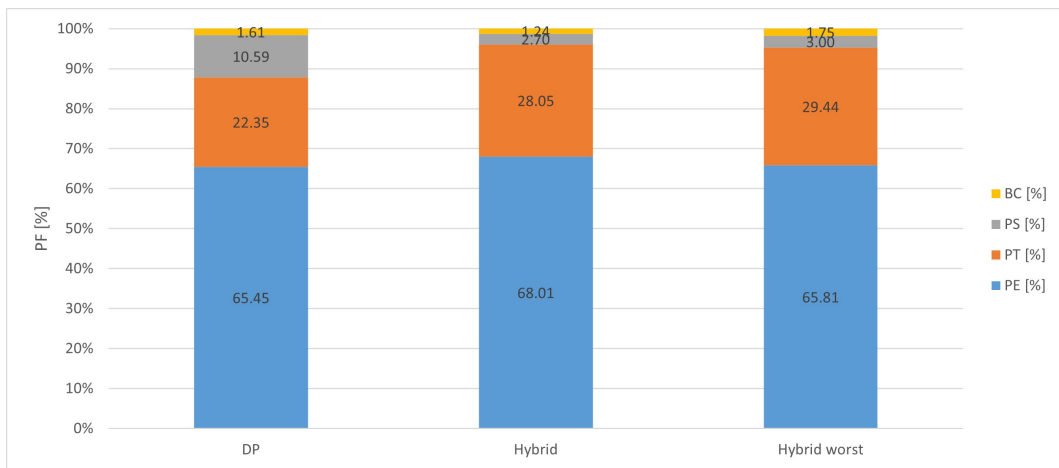


Figure 5.18: Powerflow strategies on FTP72 - Hybrid controller

5.3 JC08

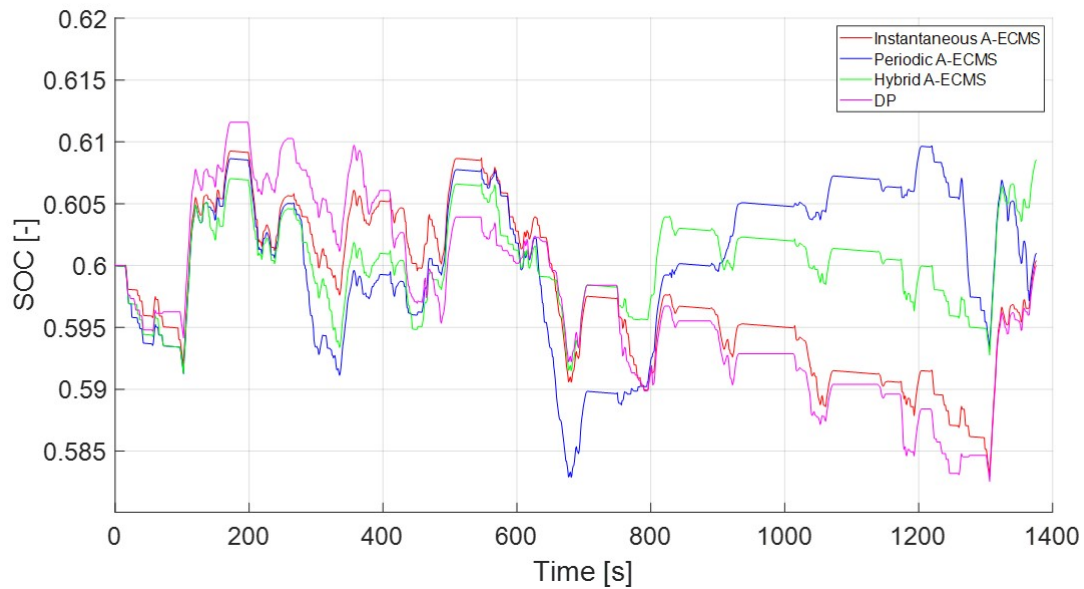


Figure 5.19: SOC profile on JC08 - Best case scenario

Quantity	Control Strategy			
	DP	Instantaneous	Periodic ($k_p=6, k_i=0.2$)	Hybrid ($k_p=6, k_i=0.2, k_v=0.005$)
$s_{chg}[-]$	-	2.1458	-	-
$s_{dis}[-]$	-	2.3776	2.2423	2.2482
$CO_{2,ttw}[g/km]$	327.33	328.40	333.07	335.97
$CO_{2,ttw,eq}[g/km]$	327.33	328.40	333.07	335.97
$FC_{ttw}[l/100km]$	12.93	12.97	13.16	13.27
$FC_{ttw,eq}[l/100km]$	12.93	12.97	13.16	13.27
$SOC_{final}[-]$	0.6000	0.6004	0.6010	0.6085
$SOC_{min}[-]$	0.5825	0.5830	0.5829	0.5912
$SOC_{max}[-]$	0.6116	0.6093	0.6097	0.6085
$\Delta CO_2\%DP$	0.000	0.3272	1.7538	2.6393
$\Delta CO_2\%PT$	-18.85	-18.59	-17.43	-16.71
ΔSOC	0.000	0.0004	0.0010	0.0085
SOC Window	0.0291	0.0263	0.0268	0.0173

Table 5.6: Best case scenario on JC08 test cycle

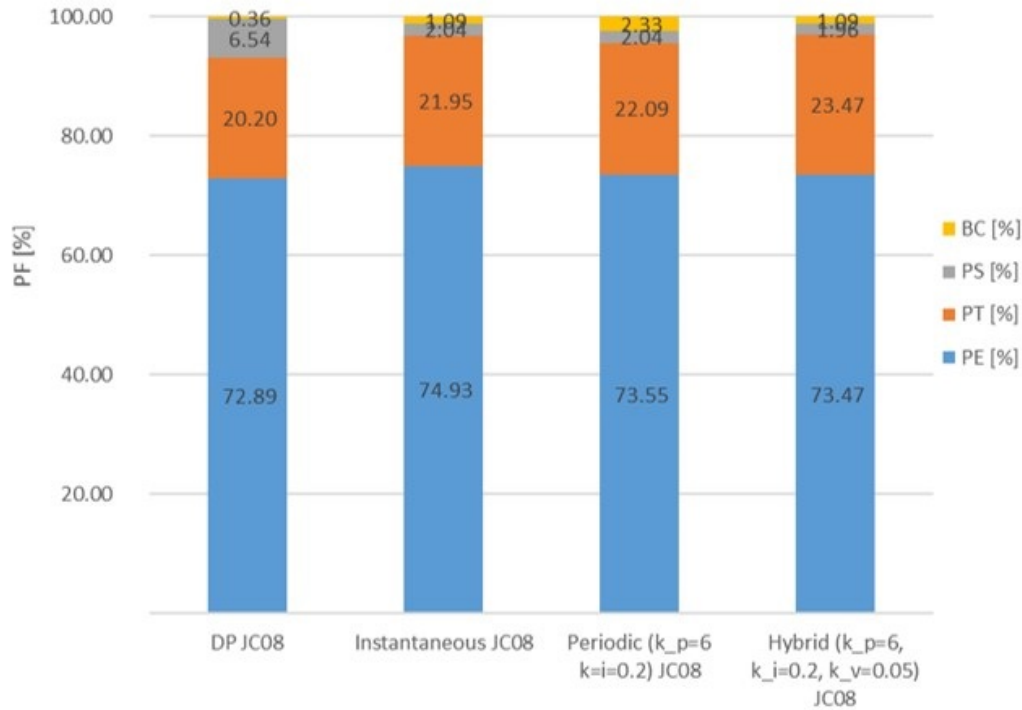


Figure 5.20: Powerflow strategies on JC08 for different controllers - Best case scenario

With reference to Figure 5.19 and results reported in Table 5.6, the controller implementation on JC08 driving cycle evidences a high level of fitting between the dynamic programming and the instantaneous formulation. This result is the child of the instantaneous update of the EF within the cycle, which makes this kind of strategy more suitable for urban mission rather than periodic ones, which are not able to adapt to sudden variation in acceleration and deceleration typical of a congested traffic context. As usual, the hybrid formulation performs better than the instantaneous one if we consider the SOC window, which is also the narrower among the controllers. This in turn would imply a better battery health in the long term horizon and a more stable behaviour of the EMS, which is able to end up the mission without strong current variation either in charge and discharge phase. Similar conclusion can be drawn by the powerflow management reported in Figure 5.20, where the higher use of the thermal unit performed with the hybrid controller leads to an higher emission with respect to the other. Similarities between the dynamic programming and the instantaneous controller are here clearly noticeable as well, stating that similar SOC profile leads to comparable EMS. As a result, the best choice for a strictly urban driving cycle could be represented by the instantaneous formulation, which performed the best mission in terms of both emission and final SOC value, even if the SOC window is not narrow as the hybrid strategy.

The choice of the instantaneous controller for a mission JC08-like, can be addressed also by looking at the charge-sustainability in terms of SOC window reported in Table 5.7 and by comparing Figures 5.22 (d) and 5.24 (d).

Quantity	Control Strategy			
	DP	Instantaneous	Periodic ($k_p=6, k_i=0.2$)	Hybrid ($k_p=6, k_i=0.2, k_v=0.005$)
$s_{chg}[-]$	-	2.4748	-	-
$s_{dis}[-]$	-	2.2248	2.3557	2.4011
$CO_{2,ttw}[g/km]$	327.33	347.23	345.88	348.90
$CO_{2,ttw,eq}[g/km]$	327.33	347.23	345.88	348.90
$FC_{ttw}[l/100km]$	12.93	13.72	13.67	13.79
$FC_{ttw,eq}[l/100km]$	12.93	13.72	13.67	13.79
$SOC_{final}[-]$	0.6000	0.6142	0.6139	0.6199
$SOC_{min}[-]$	0.5825	0.5983	0.5839	0.5871
$SOC_{max}[-]$	0.6116	0.6142	0.6153	0.6199
$\Delta CO_2\%DP$	0.000	6.08	5.67	6.59
$\Delta CO_2\%PT$	-18.85	-13.92	-14.25	-13.50
ΔSOC	0.000	0.0142	0.0139	0.0199
SOC Window	0.0291	0.0159	0.0314	0.0329

Table 5.7: Worst case scenario on JC08 test cycle

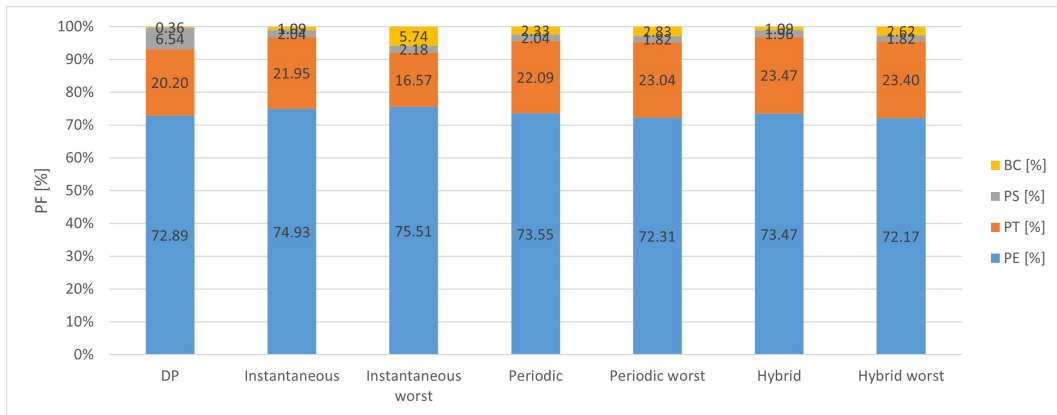


Figure 5.21: Powerflow strategies comparison on JC08

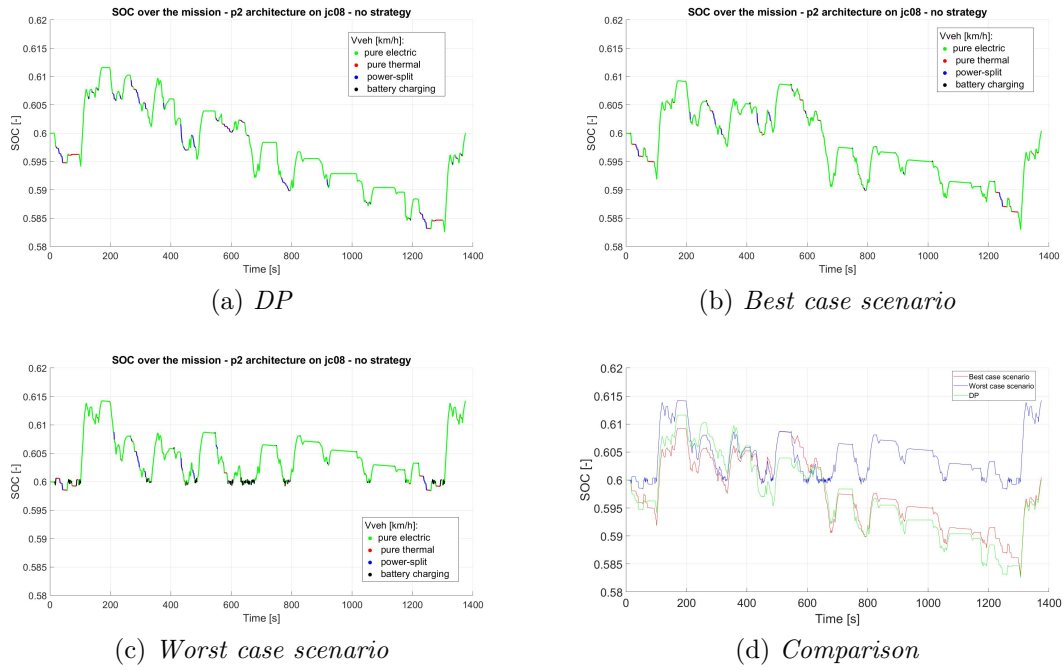


Figure 5.22: EMS comparison on JC08 - Instantaneous controller

Even in the worst case scenario (Figure 5.22 (c)) the instantaneous formulation keeps the SOC about the reference, despite the sudden torque variation requested by the cycle and the depleting trend followed by the Dynamic Programming optimizer (Figure 5.22 (a)) and the best case scenario (Figure 5.22 (b)) from the half-length of the mission.

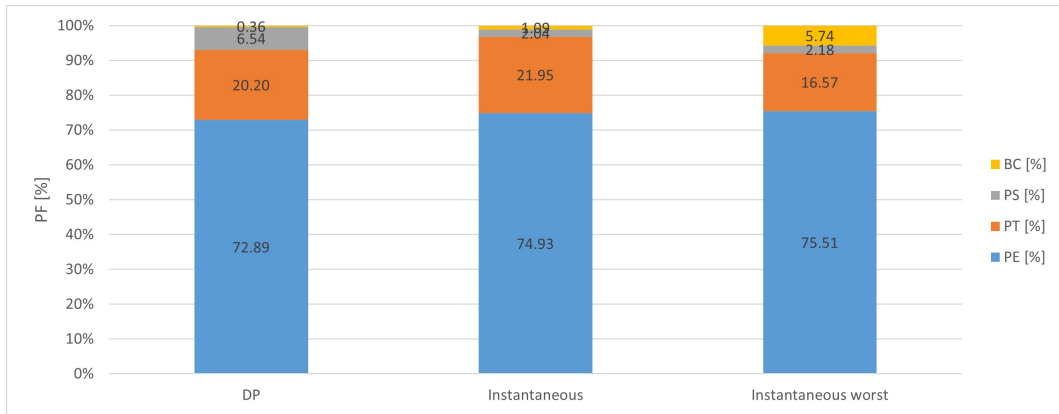


Figure 5.23: Powerflow strategies on JC08 - Instantaneous controller

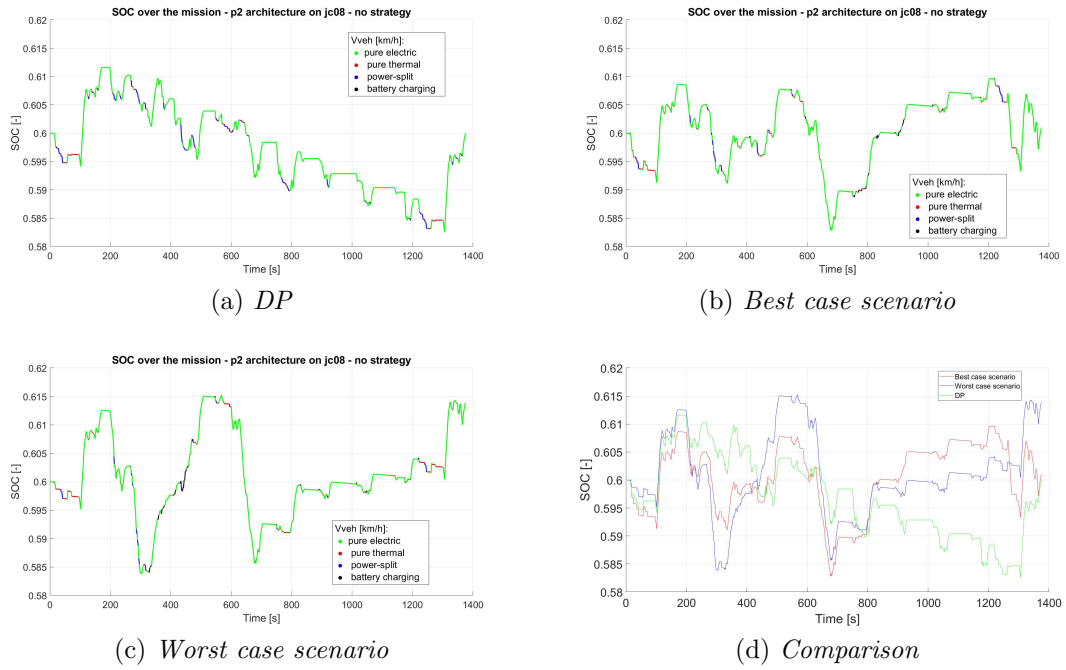


Figure 5.24: EMS comparison on JC08 - Periodic controller

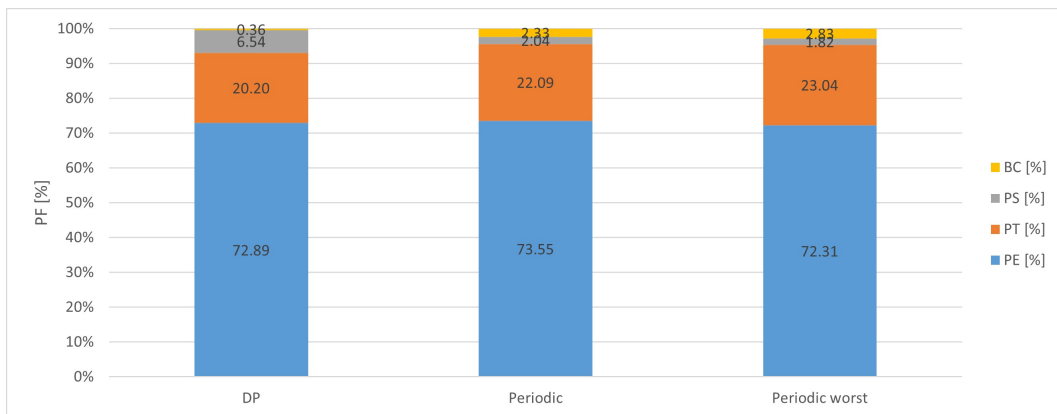


Figure 5.25: Powerflow strategies on JC08 - Periodic controller

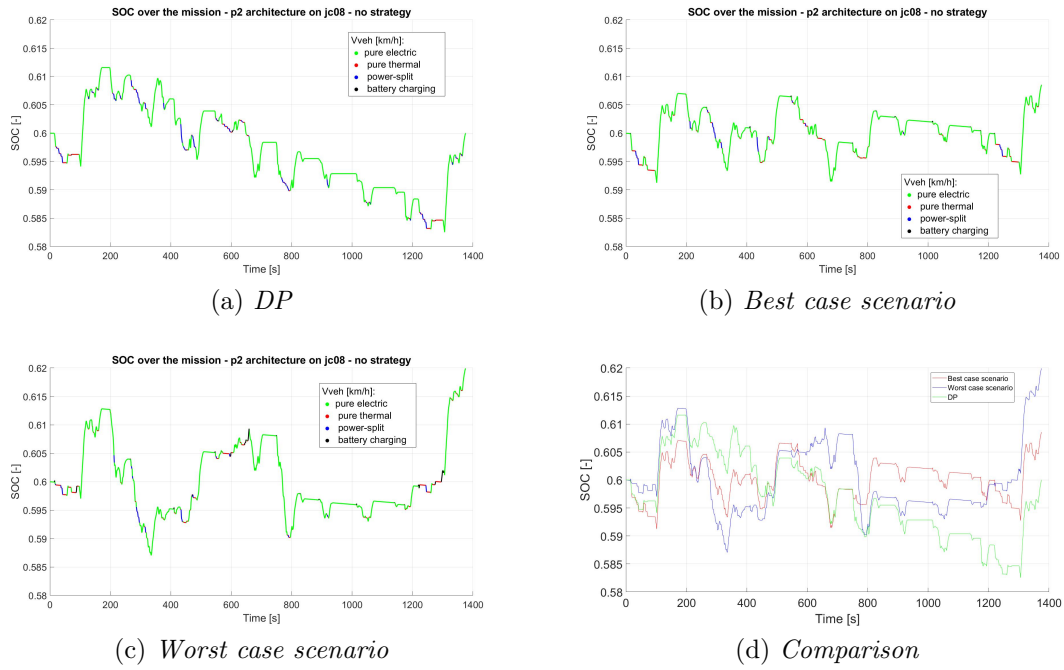


Figure 5.26: EMS comparison on JC08 - Hybrid controller

The hybrid controller, instead, performs the worst optimization both in the best and in the worst case scenario.

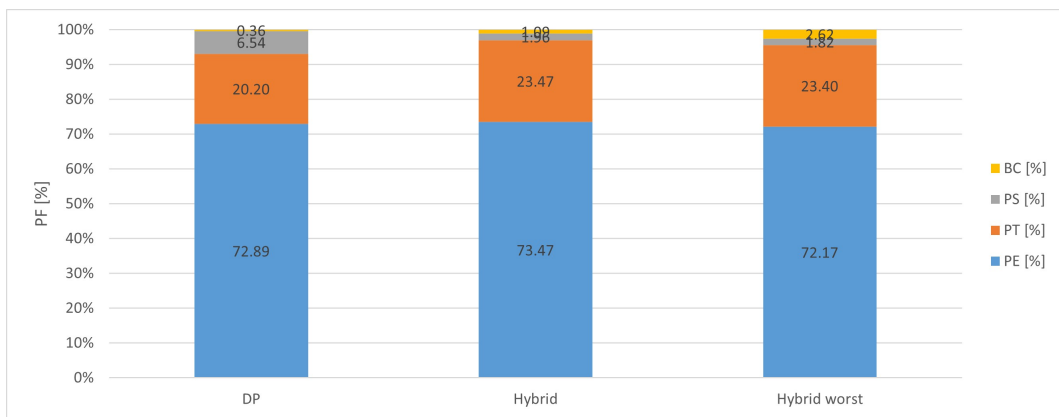


Figure 5.27: Powerflow strategies on JC08 - Hybrid controller

Chapter 6

Conclusions and Future works

6.1 Conclusions

The present work is focused on evaluating the advantages of the transformation of a conventional heavy-duty truck equipped with a 4,5L compression ignition engine into a full hybrid version by applying an Adaptive - Equivalent Consumption Minimization Strategy (A-ECMS) as instantaneous optimization method on-board implementable for the energy management strategy.

These controllers are capable of defining in real time the control variable of the control strategy, i.e. the gear number and the powerflow. The latter refers to the sequence of instantaneous operating mode - pure thermal, pure electric, power split or battery charging - that ensures the minimization of the global cost function of the optimizer. Once this cost function is correctly implemented and proper constrained are fixed for each vehicle component, the control algorithm is capable of defining the control parameters known as equivalence factor, which represent the weight attributed to the battery equivalent consumption, either in charge and in the discharge, on the whole instantaneous fuel consumption, thermal unit included -*Eqn. (2.5)*.

Given the wide range of formulation proposed in literature and to overcome the shortcomings derived from the ECMS formulation (see Chapter 2), such main logic has been applied to three different adaptive control strategy optimizer proposed in Chapter 4. The algorithms have been tested over three different driving cycles to assess their robustness and validity in multiple traffic scenarios, by stating their best and worst attitude, and compared to the benchmark given by the Dynamic Programming optimization algorithm. The main outcomes of this study have been summarized as follows.

Reduction in computational time

Considering the hardware adopted for the thesis development ¹ and the optimization tool provided [25], the computational time required to simulate the control strategy and derive the optimal control strategy for the mission is consistently reduced, passing from 10 minutes of the DP to the 8 seconds (as average) performed by the proposed controller.

¹CPU: Intel(R) Core(TM) i7-6700HQ - 2.60 GHz; RAM: 16 GB

A-ECMS and on-board implementability of the EMS

As detectable from Chapter 5, the best results have been obtained with the *instantaneous and hybrid optimization algorithms*. The former, particularly, has been demonstrated to be valid both for a mixed driving cycle and for a urban-type mission. Among the three driving cycle, it shows the major fitting with the DP optimizer with respect to the other strategies, even if the SOC window and the cycle-adaptivity is not competitive as the one performed by the hybrid formulation, which perhaps should be improved given the good results achieved. Moreover, it does not require high level of calibration and know the mission a-priori, so that it can be implemented on-board. A charge-sustaining behaviour has been always guaranteed together with a final SOC value closer to the reference, with a significant reduction in terms of emissions and not-negligible benefits in terms of fuel economy.

6.2 Future works

Adaptive Strategy based on Intelligent Traffic Systems or On-board Radar

By making reference to [14], [15] and [16], a future improvement would integrate the adaptive strategy with the traffic informations or by implementing an Adaptive Cruise Control (ACC) to assess the robustness of the controller given frontal obstacles of any kind.

Inclusion of Power Take Off (PTO) operation

Hybrid vehicles are in the position to deliver power demands from PTOs partly from recuperated energy and/or from engine operation in more favourable engine operating points. Therefore PTO power demand could be delivered by a HD Hybrid vehicle at lower specific emissions than by a conventional vehicle.

Bibliography

- [1] *Does the ICE have a future?*, SAE International Workshop, Politecnico di Torino, January 2020.
- [2] Drabik E., Rizos V., *Prospects for electric vehicle batteries in a circular economy*, CEPS, July 2018.
- [3] Bellman R., Kalaba E. R., *Dynamic programming and modern control theory*, Academic Press New York, 1965.
- [4] Musardo C., Rizzoni G., Guezennec Y., Staccia B., *A-ECMS: An Adaptive Algorithm for Hybrid Electric Vehicle Energy Management*, European Journal of Control, 2005.
- [5] Finesso R., Spessa E., Venditti M., *Robust equivalent consumption-based controllers for a dual-mode diesel parallel HEV*, Elsevier, 2016.
<https://doi-org.ezproxy.biblio.polito.it/10.1016/j.enconman.2016.08.021>
- [6] Ju F., Zhuang, L. Wang, Z. Zhang, *Optimal sizing and adaptive energy management of a novel 4WD Hybrid Powertrain*, Elsevier, 2019.
- [7] Chen H., Kessels J.T.B.A., Weiland S. , *Adaptive ECMS: a Causal Set-theoretic Method for Equivalence Factor Estimation*, Elsevier, 2015.
- [8] Sun C., Sun F., He H., *Investigating adaptive-ECMS with velocity forecast ability for hybrid electric vehicles*, Elsevier, 2016.
- [9] Yang F., Paindavoine M., *Implementation of an RBF Neural Network on Embedded Systems: Real-Time Face Tracking and Identity Verification*, ICCT, 2003.
- [10] Tian X., Cai Y., Sun X., Zhu Z., Xu Y., *An adaptive ECMS with driving style recognition for energy optimization of parallel hybrid electric buses*, Elsevier, 2019.
- [11] Zhang Y., Chu L., Fu Z., Xu N., Guo C., Zhang X., Chen Z., Wang P., *Optimal energy management strategy for parallel plug-in hybrid electric vehicle based on driving behavior analysis and real time traffic information prediction*, Elsevier – Mechatronics, 2017.
- [12] Des Buttes A. G., Jeanneret B., Kéromnès A., Le Moyne L., Pélicier S., *Energy management strategy to reduce pollutant emissions during the catalyst light-off of parallel hybrid vehicles*, Elsevier, 2020.
- [13] Grondin O., Thibault L., Quèrel C., *Transient Torque Control of a Diesel Hybrid Powertrain for NO_x Limitation*, 2012 Workshop on Engine and Powertrain Control, Simulation and Modeling - IFAC.

- [14] Zhang F , Xi J , Langari R . *Real-time energy management strategy based on velocity forecasts using V2V and V2I communications*, IEEE Trans Intell Transp Syst 2017; 18 (2):416–30 .
- [15] Taghavipour A , Vajedi M , Azad NL , McPhee J ., *A comparative analysis of route-based energy management systems for PHEVs*, Asian J Control 2016; 18 (1):29–39 .
- [16] Tian H , Li SE , Wang X , Huang Y , Tian G ., *Data-driven hierarchical control for online energy management of plug-in hybrid electric city bus*, Energy 2018; 142 :55–67.
- [17] Bosch R., *Bosch Automotive Electrics and Automotive Electronics Systems and Components, Networking and Hybrid Drive - 5th Edition*, Springer, 2007.
- [18] Picchirallo A.S.G., *Component Sizing and Real time Control using the A-ECMS method in a Parallel HEV*, McMaster University, 2019.
- [19] Onori S., Serrao L., Giorgio R., *Hybrid Electric Vehicle Energy Management Strategies*, Springer, 2016.r
- [20] Millo F., *Notes from the course in Propulsori Termici*, Politecnico di Torino, A.Y. 2019-2020.
- [21] Spessa E., *Notes from the course in Controllo delle Emissioni di Inquinanti*, Politecnico di Torino, A.Y. 2019-2020.
- [22] Genta G., *Vibration Dynamics and Control*, Chapter 11 - Controlled Linear System, Springer, 2009.
- [23] Kessels J., Koot M., van den Bosch P., Kok D., *Online energy management for hybrid electric vehicles*, IEEE Trans. Veh. Technol. 57(6), 3428–3440, 2008.
- [24] Onori S., Serrao L., Giorgio R., *Adaptive equivalent consumption minimization strategy for hybrid electric vehicles*, in Proceedings of the 2010 ASME Dynamic Systems and Control Conference, 2010.
- [25] Venditti M., *Innovative Models and Algorithms for the Optimization of Layout and Control Strategy of Complex Diesel HEVs*, 2015.
- [26] Mathworks, *Model-Based Calibration Toolbox Manual*.
- [27] Burhenne S., Henze G.P., *Sampling based on Sobol' sequences for Monte Carlo techniques applied to building simulations*, Proceedings of Building Simulation 2011: 12th Conference of International Building Performance Simulation Association, Sydney, 14-16 November.
- [28] *Global technical regulation on Worldwide harmonized Light vehicles Test Procedure - ECE/trans/180/Add.15/G.T.R. 15 regulation*, 2014.